



Sourcing and long-range transport of particulate organic matter in river bedload: Río Bermejo, Argentina

Sophia Dosch^{1,2}, Niels Hovius^{1,2}, Marisa Repasch³, Joel Scheingross⁴, Jens M. Turowski¹,
Stefanie Tofelde⁵, Oliver Rach¹, and Dirk Sachse^{1,6}

¹GFZ German Research Centre for Geosciences, Potsdam, Germany

²Institute of Geosciences, Universität Potsdam, Potsdam, Germany

³Institute of Arctic and Alpine Research, University of Colorado Boulder, Boulder, CO, USA

⁴Department of Geological Sciences and Engineering, University of Nevada Reno,
Nevada Geosciences, Reno, NV, USA

⁵Institute of Geological Sciences, Freie Universität Berlin, Berlin, Germany

⁶Department of Geography, Humboldt Universität zu Berlin, Berlin, Germany

Correspondence: Sophia Dosch (sophia.dosch@gfz-potsdam.de)

Received: 26 October 2023 – Discussion started: 13 November 2023

Revised: 3 June 2024 – Accepted: 2 July 2024 – Published: 19 August 2024

Abstract. Fluvial transport of organic carbon from the terrestrial biosphere to the oceans is an important term in the global carbon cycle. Traditionally, the long-term burial flux of fluvial particulate organic carbon (POC) is estimated using river suspended sediment flux; however, organic carbon can also travel in river bedload as coarse particulate organic matter (POM_{Bed}). Estimates of fluvial POC export to the ocean are highly uncertain because few studies document POM_{Bed} sources, flux, and evolution during long-range fluvial transport from uplands to ocean basins. This knowledge gap limits our ability to determine the global terrestrial organic carbon burial flux. In this study we investigate the flux, sources, and transformations of POM_{Bed} during fluvial transport over a ~ 1300 km long reach of the Río Bermejo, Argentina, which has no tributary inputs. To constrain sourcing of POM_{Bed}, we analyzed the composition and stable hydrogen and carbon isotope ratios ($\delta^2\text{H}$, $\delta^{13}\text{C}$) of plant wax biomarkers from POM_{Bed} at six locations along the Río Bermejo and compared this to samples of suspended sediment, soil, leaf litter, and floating organic debris (POM_{float}) from both the lowland and headwater river system. Across all samples, we found no discernible differences in *n*-alkane average chain length or *n*C29 $\delta^{13}\text{C}$, indicating a common origin for all sampled POM_{Bed}. Leaf litter and POM_{float} *n*C29 $\delta^2\text{H}$ values decrease with elevation, making it a useful proxy for POM_{Bed} source elevation. Biomarker $\delta^2\text{H}$ values suggest that POM_{Bed} is a mix of distally derived headwater and locally recruited floodplain sources at all sampling locations. These results indicate that POM_{Bed} can be preserved during transport through lowland rivers for hundreds of kilometers. However, the POM_{Bed} flux decreases with increasing transport distance, suggesting mechanical comminution of these coarse organic particles and progressive transfer into the suspended load. Our provisional estimates suggest that the carbon flux from POM_{Bed} comprises less than 1 % of the suspended load POC flux in the Río Bermejo. While this represents a small portion of the river POC flux, this coarse, high-density material likely has a higher probability of deposition and burial in sedimentary basins, potentially allowing it to be more effective in long-term CO₂ drawdown relative to fine suspended particles. Because the rate and ratio of POM_{Bed} transport versus comminution likely vary across tectonic and climatic settings, additional research is needed to determine the importance of POM_{Bed} in the global carbon cycle.

1 Introduction

The burial of organic carbon (OC) in soils and sedimentary depocenters can remove carbon from the atmosphere over timescales of centuries to millennia (Hilton and West, 2020; Galy et al., 2015; Blair and Aller, 2012; Battin et al., 2009; Hayes et al., 1999; Stallard, 1998; France-Lanord and Derry, 1997; Berner, 1982). OC buried in sedimentary basins is mainly sourced from tectonically active environments, like mountainous areas where physical erosion mobilizes hillslope bedrock and soil, generating sediment (e.g., Galy et al., 2015; Blair and Aller, 2012; Stallard, 1998). Rivers play a key role as conduits in the carbon cycle, moving OC eroded from rock, soil, and vegetation from terrestrial to marine carbon reservoirs if the transported carbon is buried in a sedimentary basin (e.g., Schlünz and Schneider, 2000). The long spatial and temporal scales of this transport allow for carbon transformation during transfer and intermittent storage (Blattmann et al., 2019; Galy et al., 2008), for instance in floodplains, estuaries, and coastal mud belts (Repasch et al., 2022; Scheingross et al., 2021; Canuel and Hardison, 2016; Aller, 1998).

It is usually assumed that once particulate organic matter (POM) from terrestrial sources has been transferred into rivers, it is transported with the fine suspended sediment (Kao et al., 2014). Estimates of POM flux, as opposed to dissolved OM, suggest that rivers deliver 110–230 Mt C into the oceans annually (Galy et al., 2015). River bedload can comprise lithic fragments that contain fossil organic carbon (J. C. Smith et al., 2013; Hage et al., 2020; Kao et al., 2014), a phase of particulate OC that might be oxidized and emit CO₂ during floodplain transit (Dellinger et al., 2023). A second organic bedload component consists of plant debris.

Particulate OM includes coarse plant material and can be abundant, ranging from 10 % up to 80 % of the total fluvial OC flux (Seo et al., 2008; West et al., 2011; Kao et al., 2014; Turowski et al., 2016). Hillslope mass wasting, overland flow, and flooding of riparian zones can mobilize leaf litter and woody debris into the fluvial routing system (Turowski et al., 2016; West et al., 2011; Wohl et al., 2009). Coarse POM can float at the river surface, where it is visible and accountable (e.g., Ruiz-Villanueva et al., 2019; West et al., 2011; Wohl et al., 2009), or it can move along the riverbed where it is more difficult to observe and measure (e.g., Turowski et al., 2013). The physical, chemical, and biological breakdown of woody debris (Seo et al., 2008) resting in the landscape allows the material to become waterlogged within days or weeks (Hoover et al., 2010). This can increase the density of organic debris above the critical value of 1.0 g cm⁻³ so that it will sink to the riverbed (Turowski et al., 2016, 2013). There, it can be transported with the bedload (e.g., Schwab et al., 2022; Hage et al., 2020; Lee et al., 2019; Turowski et al., 2016; Liu et al., 2016) and has been observed to comprise up to 75 % of all coarse POM (Turowski et al., 2016).

Several studies describe fresh, coarse terrestrial organic debris transported to delta plains (Allen et al., 1979) and offshore (West et al., 2011) by turbidity currents (Hage et al., 2020; Liu et al., 2013; Tyson and Follows, 2000). When capped by muddy siliciclastic sediments, terrestrially sourced coarse POM is protected from fast degradation (Hage et al., 2020; Lee et al., 2019; McArthur et al., 2016; Sparkes et al., 2015), leading to preservation rates of up to 70 % (Hage et al., 2022; Kao et al., 2014). Coarse woody debris and litter fragments have been described in aged deep-marine fan deposits (Lee et al., 2019) and to represent up to 12 % of the mass in exhumed turbidite layers (Turowski et al., 2016; Tyson and Follows, 2000). Taken together, these observations suggest that transport of terrestrial POM in river bedload may be a relevant pathway in the global carbon cycle (Hage et al., 2020; Lee et al., 2019; Kao et al., 2014) both during source-to-sink transit and in depocenters.

However, organic debris at the riverbed is difficult to observe and quantify due to logistical difficulties in sampling and highly variable transport rates (Turowski et al., 2013). The occurrence, recruitment, sources, and fate of POM_{Bed} during transport have only been addressed for a few headwater streams (Turowski et al., 2016, 2013; Bunte et al., 2016; Iroumé et al., 2020; Fogel and Lininger, 2023) and even less for lowland systems (Hage et al., 2022; Schwab et al., 2022). The paucity of work on the origin of POM_{Bed}, and its endurance in long-range fluvial transport after erosion, makes it difficult to build a mechanistic model to predict bedload OC fluxes and quantify their role in the terrestrial OC cycle.

In this study, we evaluate the role of organic bedload in the OC cycle of a large lowland river, the Río Bermejo in northwest Argentina. This river is a major tributary to the Río Paraguay, draining a section of the eastern central Andes across an 800 km wide foreland without overwhelming human intervention (Repasch et al., 2023). The lowland portion of the Río Bermejo has no major tributaries or distributaries over a flow distance of almost 1300 km, ruling out sediment mixing complexities inherent to dendritic drainage networks. We address three questions designed to understand the role of POM_{Bed} in the terrestrial carbon cycle: (1) is POM transported with bedload in the lowland Río Bermejo? (2) If so, what are the source areas and mechanisms for POM_{Bed} recruitment? (3) Does POM_{Bed} survive long-range transport without transformation through the Río Bermejo? To answer these questions, we collected organic-rich material traveling at the riverbed, analyzed the geochemical composition of the collected organic-rich material, and tracked compositional changes with increasing distance downstream from the headwaters.

2 Study area, sampling methods, and analyses

2.1 Study area

The Río Bermejo, with a catchment area of 120 283 km², drains the northern–western Argentinian Andes before crossing the Gran Chaco alluvial plain and joining the Río Paraguay (Fig. 1a). The Río Bermejo headwaters extend to the eastern limit of the arid Puna Plateau at an elevation of ~ 4 km. Headwater streams drain high-altitude dry grasslands, ultimately merging to form the upper Río Bermejo in the north and the Río San Francisco (a major headwater tributary of the Río Bermejo) in the south (Fig. 1). In the southern headwaters, mean annual rainfall is around 1000 mm yr⁻¹ and dense Yungas forests cover deeply weathered foothills. In the northern headwaters, the hinterland comprises the Eastern Cordillera and the sub-Andean zone with highly variable rainfall up to 1400 mm yr⁻¹ and Yungas montane forest (Fig. 1c). Steep relief and intense precipitation in these northern headwaters result in high sediment yields to the Río Bermejo.

At the Andean Mountain front, the upper Río Bermejo and the Río San Francisco merge to form the lowland Río Bermejo, a sand-bed river crossing the foreland basin. Just after the headwater confluence, the lowland Bermejo exhibits a braided morphology, with river width varying from 1–3 km. 175 km downstream of the confluence, the river transitions into a meandering channel, with migration rates from 40–80 m yr⁻¹. The channel width narrows to 170 m in the most downstream parts, towards the confluence with the Río Paraguay (Repasch et al., 2023, 2020; Sambrook Smith et al., 2016). River depth ranges between 4 and 10 m at high flow with channel depth increasing downstream (Sambrook Smith et al., 2016). The daily water discharge averages 432 m³ s⁻¹; however, the wet-season discharge of the austral summer accounts for ~ 75 % of the annual flow, with daily discharges up to 2000 m³ s⁻¹ (Golombek et al., 2021; Sambrook Smith et al., 2016). Grain size analyses show downstream fining of the suspended river load (Repasch et al., 2020) from medium sand, on average 280 µm in the headwaters, to very fine sand to silty sand, on average 90 µm in the downstream part of the river (Sambrook Smith et al., 2016; McGlue et al., 2016). The Río Bermejo delivers ~ 80 Mt yr⁻¹ of suspended sediment to the Río Paraguay. Suspended sediment input from the Andean headwaters at the Bermejo–San Francisco confluence is significantly higher at ~ 103 Mt yr⁻¹, suggesting net deposition during foreland transit (Repasch et al., 2020). The Río San Francisco contributes ~ 14 % to the total suspended sediment load of the Río Bermejo main stem, whereas the northern headwaters contribute ~ 86 % (Repasch et al., 2020), likely reflecting the south-to-north gradient in precipitation, vegetation, and erosion rate.

Our work is focused on the Río Bermejo downstream of the eastern Andean Mountain front, from the confluence of the Río Bermejo and the Río San Francisco at 304 m a.s.l.

to the Río Bermejo–Río Paraguay confluence at 50 m a.s.l. The linear distance between these points is ~ 700 km, while the river has a channel length of ~ 1300 km due to its high sinuosity. Over this distance, no significant tributaries join the Río Bermejo, making it an ideal setting for our source-to-sink study of organic bed material.

2.2 Sampling

During sampling campaigns in 2013, 2015, 2017, 2019, and 2020, we collected headwater and lowland floodplain leaf litter, coarse floating particulate organic matter (POM_{float}, > 1 cm diameter), soils from dry paleo-channels, riverbank sediments, suspended sediment, and bedload material in the Río Bermejo catchment (Table 1, Fig. 1a). Sampling of bedload was curtailed by pandemic travel restrictions coming into force during fieldwork in March 2020.

The sampling sites at Río Colorado and Embarcación are located within the northern headwaters (HW_{North}), and Caimancito and Pichanal are sampling sites in the southern headwaters (HW_{South}) along the Río San Francisco (Fig. 1a). We sampled the Río Bermejo main stem at five separate locations between the most upstream location at Carboncito (14 km linear distance downstream of the mountain front confluence) and the most downstream site at General Mansilla (660 km linear distance downstream of the mountain front confluence) (Fig. 1, Table 1).

2.2.1 Bedload sampling: POM_{Bed}

In March 2020, we collected bedload material from cross-channel transects (Fig. 2a) at four locations upstream of the Bermejo–San Francisco confluence. At HW_{South}, we sampled the Río San Francisco at Pichanal (HW_{South-1}, $n = 13$) and at Caimancito (HW_{South-2}, $n = 2$). At HW_{North}, we sampled the upper Río Bermejo at Embarcación (HW_{North-1}, $n = 10$) and the Río Colorado tributary (HW_{North-2}, $n = 4$) (Fig. 1). Downstream of the confluence, we sampled the lowland Río Bermejo main stem at Puerto Lavalle (LL₁, $n = 12$), 481 linear kilometers (865 km streamwise) downstream of the confluence, and at El Colorado (LL₂, $n = 8$), 583 linear kilometers (1046 km streamwise) downstream of the confluence (Table 1).

We collected bedload samples with a Helley–Smith bedload sampler with a 100 µm mesh and an 8 cm × 8 cm square opening (KC Denmark A/S, 2023). We ballasted the sampler with a 12 kg weight to enable sinking to the riverbed and attached a rope to both ends of the sampler. We deployed the device systematically from bridges across the Río Bermejo and Río San Francisco, where possible multiple times along a transect (Fig. 2a). We lowered the sampler to touch gently on the riverbed for 60 s and then manually pulled it up as quickly as possible, usually in less than 15 s, to minimize capture of material from shallower water column depths. We additionally collected bedload samples at one location per sampling

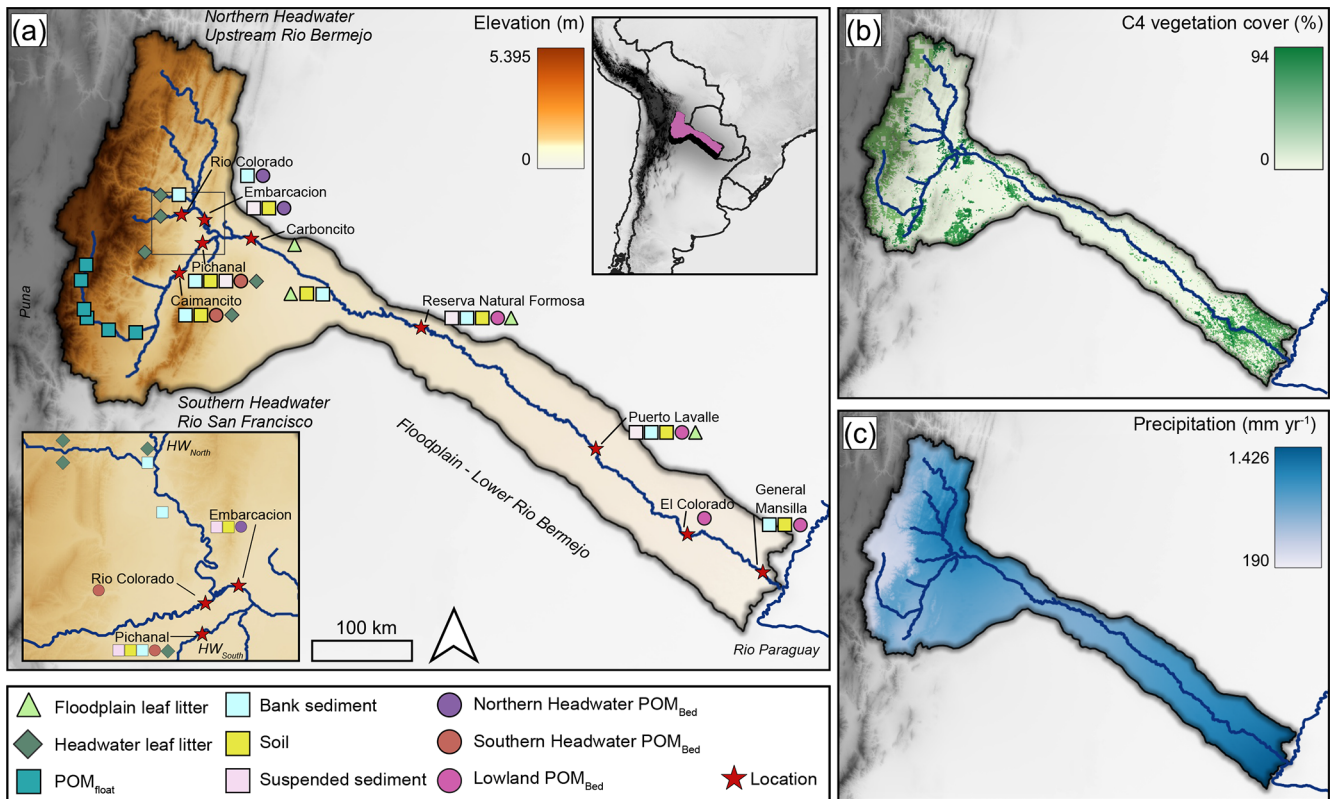


Figure 1. Catchment overview of the Río Bermejo main stem and main headwater tributaries. (a) Topographic map (ASTGTM, NASA EOSDIS Land Processes DAAC, 2019) with sample types indicated at each sampling location. Top right: catchment location in Argentina. Bottom left: zoomed-in view of the tributary confluence at the mountain front. (b) C4 vegetation cover as a percentage of total C3 and C4 vegetation cover (Powell et al., 2012). (c) Average annual precipitation rate (Hijmans et al., 2005).

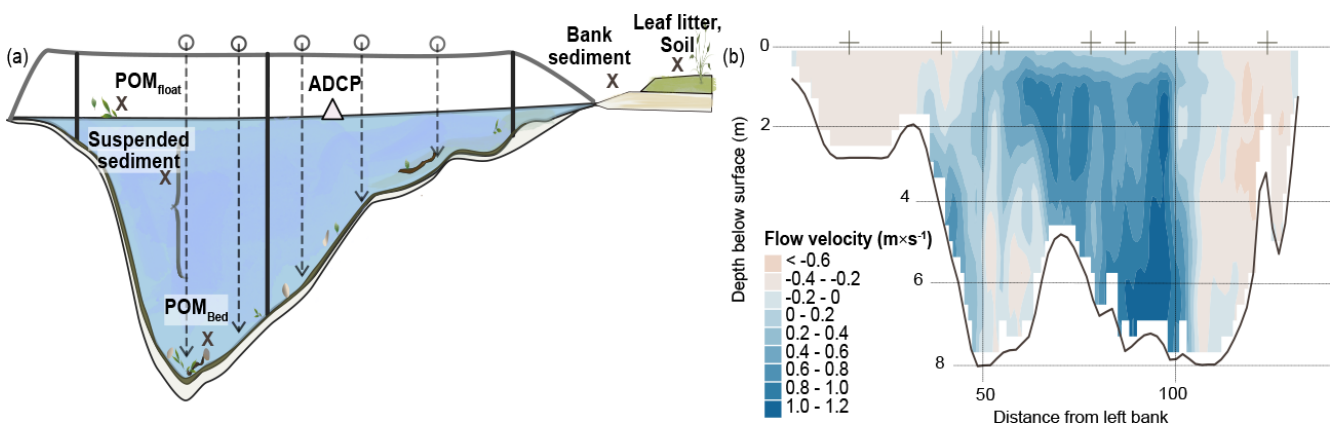


Figure 2. (a) Schematic channel cross-section with transect sampling points (arrows), sample types used in this study, and indicated sample locations. (b) Cross-channel velocity profile using an acoustic Doppler current profiler at the LL₂ station, with crosses indicating each transect sampling point at the station. Bridge pillars were at 30, 75, and 125 m, and measurements were taken ~ 5 m downstream of the bridge.

site for a longer period, usually around 5 min, to attempt the collection of a sufficient amount of organic bedload material for compositional analysis. The wet samples were stored in airtight Whirl-Pak plastic bags and transferred to Pots-

dam, Germany, within 2 weeks. The samples were freeze-dried and dry-sieved over a stainless-steel sieve with 1 mm mesh size. Of the 49 bedload samples collected in 2020, 30 yielded no or less than 1 g of macroscopic organic material

Table 1. Overview of the bedload sampling sites, location, number of samples, and type of sampling.

Location ID	Location name	Latitude	Longitude	Bermejo catchment	Distance from mountain front (km)	Year	<i>n</i>	Sample type
AR20SD01	Caimancito HW _{South-2}	−23.7109	−64.5366	Southern Headwater Río San Francisco	−22	2020	2	Transect
AR20SD05	Río Colorado HW _{North-2}	−23.2962	−64.2191	Northern Headwater Upper Río Bermejo	−16	2020	4	Transect
AR20SD02	Embarcación HW _{North-1}	−23.2479	−64.1375	Northern Headwater Upper Río Bermejo	−10	2020	4	Transect
AR20SD03	Pichanal HW _{South-1}	−23.3559	−64.1827	Southern Headwater Río San Francisco	−15	2020	13	Transect
AR17MR30	Pichanal	−23.3559	−64.1827	Southern Headwater Río San Francisco	−15	2017	1	Single point
AR17MR17	Reserva Natural Formosa	−24.3058	−61.8345	Downstream Río Bermejo	249	2017	1	Single point
AR20SD15	Puerto Lavalle LL ₋₁	−25.6654	60.1282	Downstream Río Bermejo	481	2020	12	Transect
AR20SD18	El Colorado LL ₋₂	−26.3444	−59.3614	Downstream Río Bermejo	584	2020	8	Transect
AR17MR57	El Colorado	−26.3444	−59.3614	Downstream Río Bermejo	584	2017	1	Single point
AR17MR05	General Mansilla	−26.6613	−58.6314	Downstream Río Bermejo	660	2017	1	Single point

(POM_{Bed}), many from downstream sampling sites. For selected samples with abundant organic debris in both fractions, we processed and analyzed the organic bedload material following the protocol described in Sect. 3.2 for both the > 1 mm and < 1 mm size fractions separately. We found no significant differences between the two size fractions and therefore analyzed the remaining bedload samples as bulk.

In earlier sampling campaigns, we collected individual bedload samples throughout the catchment (Table 1): in March 2017, we collected single-point bedload samples with a self-built device at one headwater site, HW_{South} (Pichanal, Río San Francisco), and three main-stem Río Bermejo sites: Reserva Natural Formosa, El Colorado, and General Mansilla (Fig. 1a). In November 2019, six bedload samples were collected with a bedload grab that did not yield enough OM to permit compound-specific stable isotope measurements or significant amounts of POM_{Bed}. The sampling in these earlier campaigns was performed for the qualitative assessment of POM_{Bed} occurrence, and corresponding data were not used to quantitatively estimate POM_{Bed}.

For our purpose, we define POM_{Bed} as organic material that is entrained within the clastic bedload, transported as separate layer on top of the clastic bedload, or moves close to the riverbed. It is likely that the POM_{Bed} material is trans-

ported in a more extensive layer above the bed (Repasch et al., 2022; Schwab et al., 2022), also including saltating trajectories (Einstein et al., 1940; Turowski et al., 2010). The maximum particle size of the bedload samples was likely limited by the funnel opening width of 8 cm, as has been demonstrated for clastic bedload (Bunte et al., 2008), and our sample collection was restricted to the material transported within 8 cm above the bed. Our sample sizes may reflect these limitations of bedload sampling rather than a physical phenomenon. We assume, however, that these potential sampling biases do not affect the composition of the sample material.

2.2.2 Leaf litter and POM_{float}

During campaigns in 2015, 2019, and 2020, we collected 17 leaf litter samples within the floodplain ranging in elevation from 138 to 271 m a.s.l. and 11 leaf litter samples from HW_{North} and HW_{South} upstream of the Río Bermejo–Río San Francisco confluence between 317–854 m a.s.l. (Fig. 1). We typically collected ~ 20 g of leaf litter; the samples were air-dried in the field and stored in paper bags upon arrival at the laboratory in Potsdam, Germany. There, the samples were

oven-dried at 40 °C for up to 3 d and stored until further analysis.

We collected seven samples of floating, coarse particulate organic matter (POM_{float}, > 1 mm) along the Río San Francisco (between 313 and 2458 m a.s.l.) during the high-flow season in March 2013 (Fig. 1a). These samples were collected with a net with mesh size 1 mm and held into the river water from the riverbanks until a sufficient amount of organic material was accumulated and contained organic and inorganic debris ranging from 1 mm to 10 cm. The sample material was stored in plastics bags and freeze-dried upon return to the laboratory. The dry sample masses ranged from 5 to 40 g.

2.2.3 Soil, bank, and suspended sediment

During campaigns in 2019 and 2020, we collected 15 sediment and 24 soil samples from the riverbanks and from a paleo-channel on the Río Bermejo megafan at elevations of ~ 60 to 390 m a.s.l. We used a rinsed, stainless-steel shovel to collect material from 0 to 20 cm below the surface. The samples were stored in paper bags and air-dried in the field. Upon returning to the laboratory, we oven-dried all samples at 40 °C for up to 3 d and transferred them into brown glass bottles before analysis. We also include data on suspended sediment particulate organic carbon abundance and composition in the Río Bermejo from previous studies (Repasch et al., 2021, 2022). Briefly, 48 samples were collected from several locations spanning HW_{South}, HW_{North}, and the lowland Río Bermejo (Fig. 1a).

3 Methods: analysis and data treatment

3.1 Near-bed flow velocity and channel depths

During the 2020 campaign, we determined the flow velocity and channel depth at the sampling locations HW_{North-1} and HW_{South-1} near the confluence and downstream at LL₋₁ and LL₋₂. Surveys were conducted from bridges using an acoustic Doppler current profiler (ADCP; SonTek RiverSurveyor RS-M9). The ADCP was mounted on a floating board and towed by a rope from the bridges. We applied strong tension to the rope in an effort to prevent the ADCP from being submerged under the bridge. Where possible and necessary, the ADCP float was guided by a person in the water. The raw ADCP data were processed using the SonTek RiverSurveyor Live Software (Version 4.1). After quality assessment with the SonTek software, we further processed the data files using the velocity mapping toolbox (v.4.09) (Parsons et al., 2013) to calculate smoothed mean cross-sections with the river flow velocity determined at horizontal and vertical grid node spacings of 1 and 0.5 m, respectively. We extracted the river depth and flow velocity at each bedload sampling point by overlaying our GPS data points with these cross-sections. To approximate the bedload transport velocity, we multiplied

the depth-averaged streamwise flow velocity from the ADCP velocity profiles by 0.7 (Chatanantavet et al., 2013).

The ADCP-estimated near-bed flow velocity ranged between -0.17 – 1.19 m s⁻¹ and was on average 0.5 ± 0.4 m s⁻¹ for the ensemble of sampling sites ($n = 4$). We attribute occasional negative flow velocities to local flow patterns on large river bedforms (Allen, 1968) and assign no general significance to them (Fig. 2b). River depths measured during the wet season varied between 8.1–8.5 m at HW_{South-1} and HW_{North-1}, 1.9–9.9 m at LL₋₁, and 2.4–8.4 m at LL₋₂. Due to the interrupted campaign in March 2020, these values do not cover the braided section of the river in the upper part of the eastern Andean foreland.

The high flow velocities and water depths of the Río Bermejo made clean sampling of river bedload difficult, and the composition of some samples may have been affected by admixture of suspended load during sampler recovery. This is most likely to occur in the sediment-laden upper reaches of the Río Bermejo and at downstream sites where bridge pillars cause additional turbulence.

3.2 Organic–geochemical analysis

To fingerprint source areas of the OM collected in this study, we use biomarker proxies, specifically long-chain *n*-alkanes, recalcitrant organic molecules that are often preserved in sediments (e.g., Thomas et al., 2021; Cranwell, 1972). Long-chain *n*-alkane stable carbon and hydrogen isotopes incorporate local environmental conditions at formation and can therefore help to track the source areas of POM in river sediment (e.g., Hemingway et al., 2016; Hoffmann et al., 2016; Bouchez et al., 2014; Ponton et al., 2014; Galy et al., 2011; Sachse et al., 2004).

We extracted *n*-alkanes from all samples and measured the compound-specific stable hydrogen and carbon isotope ratios. Soil, bank sediment, suspended sediment, and POM_{Bed} samples were ground with a mortar and pestle and lipid compounds were extracted with 9 : 1 methanol : dichloromethane using a Thermo Fisher Dionex Accelerated Solvent Extraction system (ASE 350). The non-polar *n*-alkane fraction was separated from the total lipid extract over silica gel columns with glass-fiber filters at the base and top (pore size 60 Å, 230–400 mesh particle size) by automated solid-phase extraction (SPE) with a Gilson ASPEC GX-271 and *n*-hexane as a solvent, following procedures described by Rach et al. (2020). *n*-Alkanes were extracted manually from leaf litter and POM_{float} by immersing between 0.2 and 10.0 g of the dried samples in a 9 : 1 methanol : dichloromethane mixture and placing them into an ultrasonic bath at 40 °C for 20 to 40 min. The *n*-alkanes were separated from the total liquid extract by solid-phase extraction (SPE) over a silica-gel-equipped 6 mL glass column (Macherey-Nagel, Düren, Germany) using *n*-hexane as a solvent (Rach et al., 2020). The solid parts stayed behind and samples were rinsed properly with 9 : 1 DCM/MeOH. The lipid-containing solvents

were dried in the TurboVap and the lipids were transferred to a smaller vial in approximately 1.5 mL 9 : 1 DCM/MeOH. The solvents of the total liquid extract (TLE) were evaporated again with N₂ gas and the samples were dissolved in 1.5 mL *n*-hexane. To quantify *n*-alkane concentrations per sample, we added an internal standard, 5 α -androstane (10 μ g), and measured the samples in an Agilent gas chromatograph (GC 7890-A) with a flame ionization detector (FID) and a coupled single quadrupole mass spectrometer (MS 5975-C).

We quantified the abundances of *n*-alkane homologues relative to the internal standard using the FID chromatograms. We calculated the average chain length (ACL_{25–33}) of the most abundant *n*-alkanes with chain lengths between 25 and 33 as

$$\text{ACL}_{25-33} = \frac{\sum(C_n \times n)}{\sum C_n}. \quad (1)$$

n is the number of carbon atoms of each *n*-alkane, and *C_n* is the concentration of each *n*-alkane with *n* carbon atoms. The subscripts in ACL_{25–33} refer to the chain length range analyzed.

We determined the carbon preference index (CPI_{25–33}) after Bray and Evans (1961) for *n*-alkanes with 25 to 33 carbon atoms using

$$\text{CPI}_{25-33} = \frac{1}{2} \times \left(\frac{\sum C_{25-33\text{odd}}}{\sum C_{24-32\text{even}}} + \frac{\sum C_{25-33\text{odd}}}{\sum C_{26-34\text{even}}} \right). \quad (2)$$

$\sum C_{25-33\text{odd}}$ is the sum of the concentration of odd-chained *n*-alkanes with chain lengths between 25–33, $\sum C_{24-32\text{even}}$ is the sum of the concentration of even-chained *n*-alkanes with chain lengths between 24–34, and so forth.

To measure compound-specific hydrogen and carbon isotope ratios of the *n*-alkanes (expressed as $\delta^2\text{H}$, $\delta^{13}\text{C}$ values), we used a Trace GC 1310 (Thermo Fisher Scientific) connected to a Delta V Plus isotope ratio mass spectrometer (IRMS) (Thermo Fisher Scientific), following the procedures described by Rach et al. (2020). *n*-Alkane $\delta^2\text{H}$ and $\delta^{13}\text{C}$ values were measured in duplicates. For each sample run, we measured the *n*-alkane standard mix A6 (with *n*-alkane chain lengths ranging from *n*C₁₆–*n*C₃₀) with known $\delta^2\text{H}$ values obtained from Arndt Schimmelmann (Indiana University) for correction and transfer to the VSMOW scale. The H3+ factor from the ²H measurements was 5.9 ± 0.8 mV. The standard deviation for $\delta^2\text{H}$ of the standard measurements was $2.3\text{‰} \pm 0.7\text{‰}$, and the mean standard deviation for the samples was $1.1\text{‰} \pm 1.6\text{‰}$. The mean standard deviation for ¹³C measurements of the standard measurements was $0.11\text{‰} \pm 0.06\text{‰}$, and the mean standard deviation for the samples was $0.15\text{‰} \pm 0.23\text{‰}$.

Organic–geochemical raw results

We calculated the ACL_{25–33} index for 201 samples collected in the Río Bermejo catchment, including POM_{Bed}, leaf litter,

POM_{float}, soil, sediment deposits, and river suspended sediment. *n*-Alkanes with chain lengths ranging from *n*C₂₅–*n*C₃₅ had the highest abundance across all samples (Fig. 3a–f). The main components were *n*C₃₁, *n*C₂₉, and *n*C₂₇, followed by *n*C₃₃ and *n*C₂₅, while even-carbon-numbered *n*-alkanes were minor components in all samples. Leaf litter, POM_{Bed}, and soil samples had similar concentrations of *n*C₂₉ and *n*C₃₁. In riverbank and suspended sediment samples, *n*C₃₁ was the dominant *n*-alkane, whereas *n*C₂₇ was the main component of the POM_{float} samples. We measured the $\delta^2\text{H}$ and $\delta^{13}\text{C}$ values for the dominant chain lengths, *n*C₂₉ and *n*C₃₁. Because these *n*-alkanes showed a significant correlation for $\delta^{13}\text{C}$ ($R^2 = 0.95$, $p < 0.01$) and $\delta^2\text{H}$ values ($R^2 = 0.81$, $p < 0.01$, Fig. 3g and h), we will focus on the *n*C₂₉ values.

For a subset of 10 POM_{Bed} samples with abundant organic debris in both the > 1 mm and < 1 mm fractions (HW_{South-1}, HW_{South-2}, HW_{North-1}, HW_{North-2}, LL₋₁, LL₋₂), we analyzed the *n*-alkane composition of POM_{Bed} in both size fractions. In most of these samples, the two size fractions had distinct ACL_{25–33}, CPI_{25–33}, *n*C₂₉ $\delta^2\text{H}$, and *n*C₂₉ $\delta^{13}\text{C}$ values (Fig. S1 in the Supplement). However, no discernible pattern emerged in these differences. For this reason, and because size-specific biomarker analyses were not possible for smaller sample amounts, we decided to work with *n*-alkane data from the bulk sample material. For samples analyzed as two separate fractions, we determined values for the bulk sample material as the weighted average of the two fractions. These values are dominated by the fraction < 1 mm, which had the greater mass in all cases. In the following, we will refer to the results of analyses of the total particulate organic carbon of the sampled bedload material in the full size range as POM_{Bed}.

3.3 Data analysis

All data analyses were performed using R 4.1.2 GUI 1.77 High Sierra build (8007). We report the range of the values as average \pm standard deviation and the number of samples. We used the Kolmogorov–Smirnov test to account for the non-normal distribution of our data and the Mann–Whitney *U* test to test for significant differences between independent sample groups. We used linear regression and associated R^2 values to test for significant trends in our data. Significance levels are reported at the 95 % confidence interval (p value < 0.05).

4 POM_{Bed} presence, source, and ability to survive long-distance transport

We aim to answer questions regarding the source, transport, and survival of POM_{Bed} in the Río Bermejo. First, we want to observe when and where POM_{Bed} is in active fluvial transport and how POM_{Bed} composition varies throughout the catchment. We then investigate the sources of POM_{Bed} by determining the elevation and climate of the OM source us-

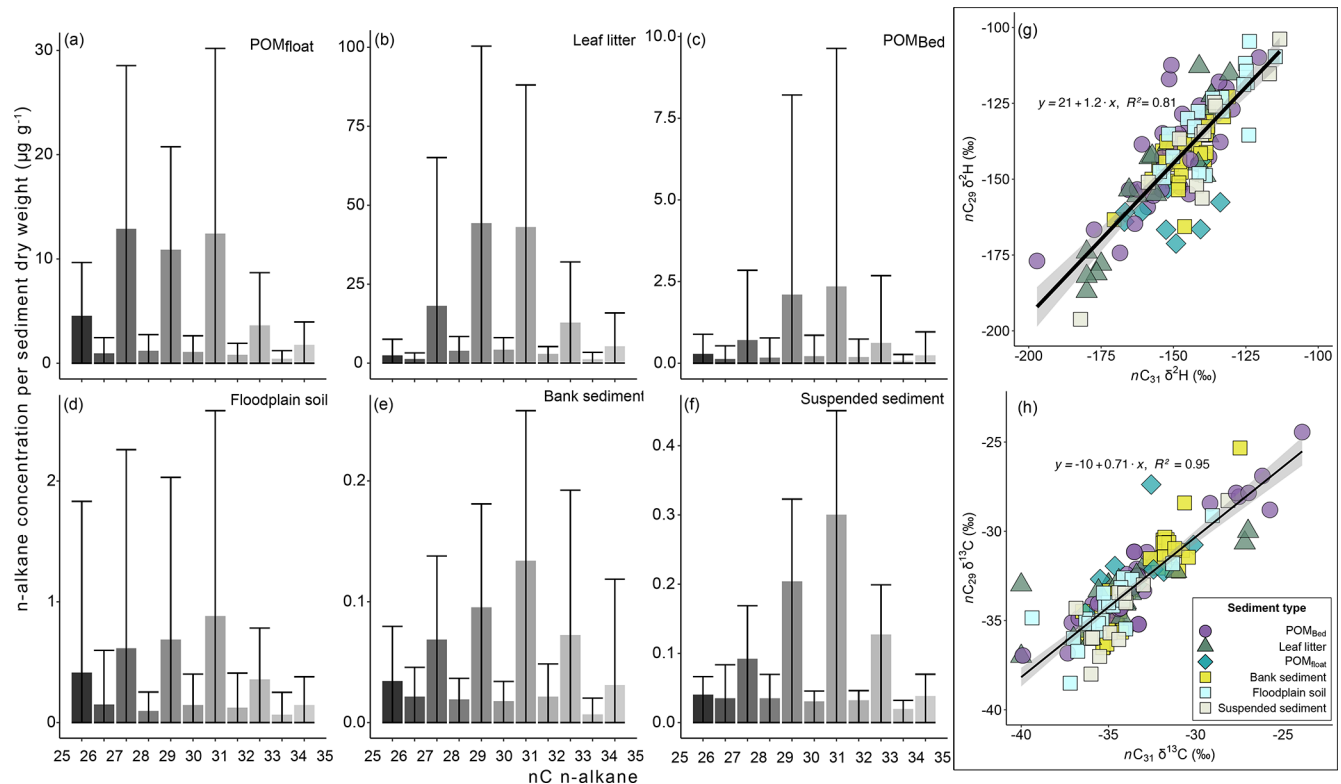


Figure 3. Left panels (a–f): average and standard deviation (bars and whiskers) of the long-chain *n*-alkane distribution (nC_{25} – nC_{35}) as the concentration per sediment dry weight ($\mu\text{g g}^{-1}$) of (a) POM_{float}, (b) leaf litter, (c) POM_{Bed}, (d) floodplain soil, (e) bank sediment, and (f) suspended sediment. Note the different y-scale ranges. Right panels (g, h): nC_{29} versus nC_{31} *n*-alkane (g) $\delta^2\text{H}$ and (h) $\delta^{13}\text{C}$ values of all OM sample types, as well as the linear regression equation and R^2 values.

ing the *n*-alkane $\delta^2\text{H}$ value, assess the biological variability of POM_{Bed} sources using $\delta^{13}\text{C}$ values combined with ACL_{25–33}, and estimate POM_{Bed} maturity using CPI_{25–33}. Finally, we apply a mixing model using these geochemical data to define distinct POM_{Bed} sources. Collectively, this approach allows us to evaluate the survival and fate of POM_{Bed} during long-range fluvial transport in the Río Bermejo.

4.1 Is there transport of POM_{Bed} in the lowland Río Bermejo, and what is its geochemical composition?

4.1.1 Bedload mass and material composition

The mass of bedload samples comprising organic and clastic particles was up to an order of magnitude greater at the headwater sites than at the downstream sites for the same sampling procedure. Sampling at HW_{South-1} and HW_{North-1} yielded totals of 560 g min^{-1} ($n = 13$) and 259 g min^{-1} ($n = 10$), respectively, while at LL₁ we collected a total of 51 g min^{-1} ($n = 12$) and at LL₂ 77.1 g min^{-1} ($n = 8$), respectively (Fig. 4d). The mass of dry POM_{Bed} in individual bedload samples varied from 0 to $\sim 20 \text{ g}$, without clear spatial patterns. The mass of organic bedload scaled loosely with the amount of clastic sediment collected (Fig. 4d), but

there was no correlation of the collected material and near-bed velocities. The material collected in POM_{Bed} samples ranged from fragile, intact leaves and twigs to robust wood fragments with frayed edges and organo-clastic aggregates in the size range from $< 1 \text{ mm}$ to $\sim 10 \text{ cm}$, often mixed with fine organic debris $< 1 \text{ mm}$ (Fig. 4). The organo-clastic aggregates were easily dissociated during sieving, separating into fine sand and silt, and apparently degraded OM particles ranging from $< 1 \text{ mm}$ to $> 1 \text{ cm}$ (Fig. 4).

Chemical maturity of an OM sample can be expressed with the CPI_{25–33}, where lower values indicate a higher sample maturity due to chemical alterations of the OM. The strong predominance of odd-over-even *n*-alkane chain lengths in POM_{Bed} (CPI_{25–33} average: 7.4 ± 3.0 , $n = 39$, Fig. 5) and the ACL_{25–33} averaging 29.6 ± 0.9 (range: 27.4–31.6, $n = 39$, Fig. 5) throughout the catchment indicate relatively fresh or little-degraded vascular plant material in the Río Bermejo bedload (Eglinton and Hamilton, 1967; Bray and Evans, 1961). The occurrence of low CPI_{25–33} < 1 values in our dataset may be due to the occasional presence of burned OM, such as charcoal particles, in the river bedload. While it is difficult to evaluate the volumetric contribution of this low-CPI_{25–33} material, it is negligible relative to other POM_{Bed} sources.

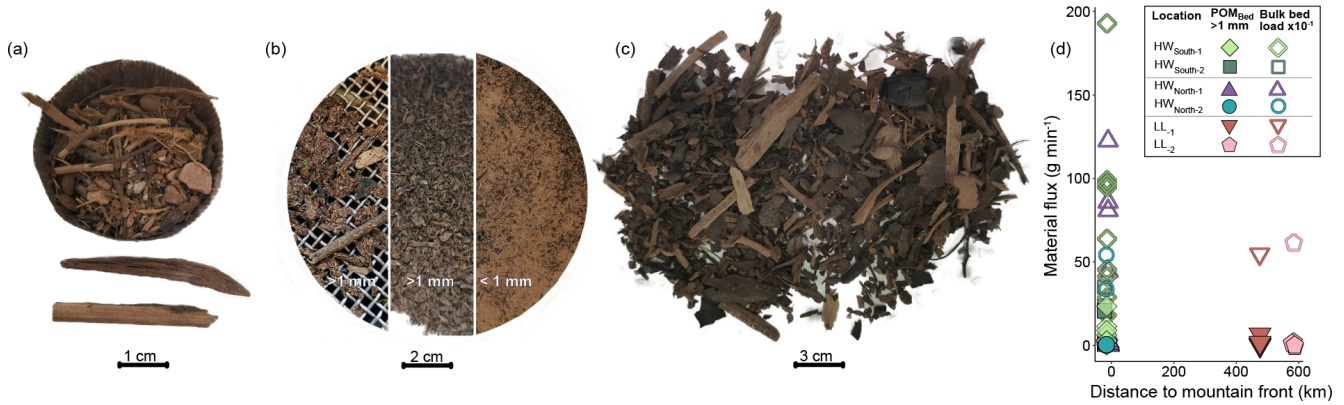


Figure 4. Examples of captured POM_{Bed} as a (a) bulk fraction from the Río San Francisco at $HW_{South-1}$ and (b) Río Bermejo at LL_1 in particle size separates: $> 1\text{ mm}$ aggregated (left) and dissociated (middle) as well as $< 1\text{ mm}$ mixed with clastic material. (c) Bulk at the Río Bermejo at $HW_{North-1}$ and (d) sampled bulk bed material (empty symbols) and $POM_{Bed} > 1\text{ mm}$ (filled symbols) per sampling point at all sampling locations. Note that $POM_{Bed} > 1\text{ mm}$ is shown in g min^{-1} and bulk bed material in $\text{g min}^{-1} \times 10^{-1}$ to account for the mass difference of the samples.

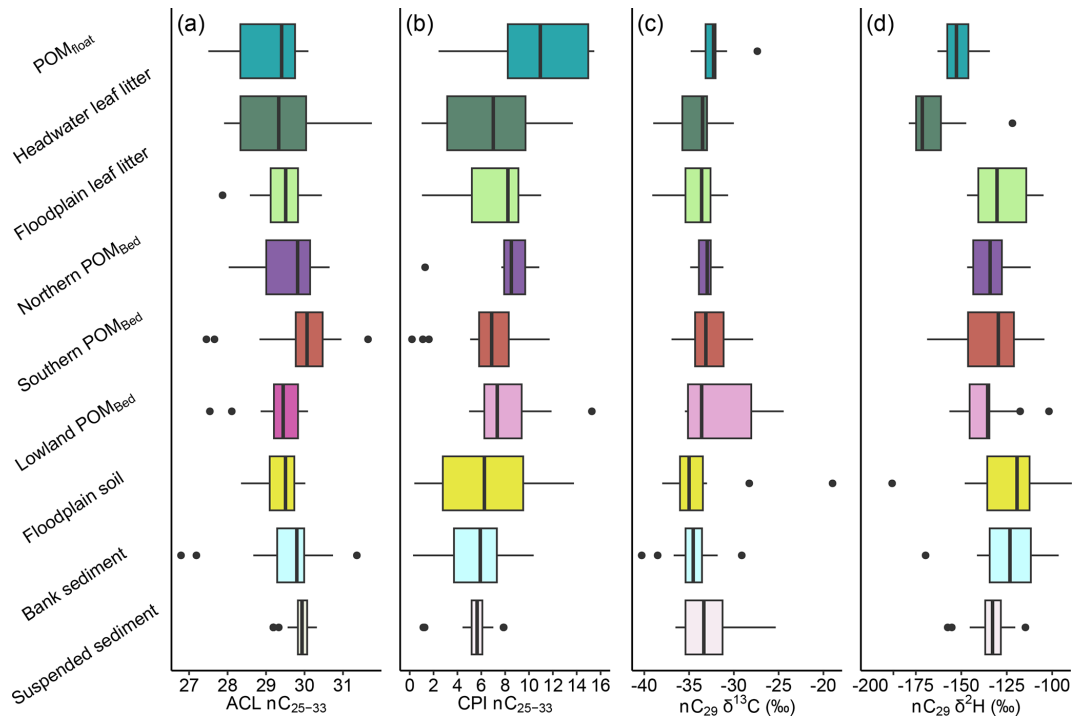


Figure 5. Summary of (a) ACL_{25-33} , (b) CPI_{25-33} , (c) $nC_{29} \delta^{13}C$, and (d) $nC_{29} \delta^2H$ values of POM_{float} from headwater and floodplain leaf litter. POM_{Bed} from the northern headwater, southern headwater, downstream floodplain, floodplain soil, bank sediment, and suspended sediment. The box plot width shows the interquartile range, with the black line showing the median and the whiskers the minimum and maximum range of the data without outliers. Black dots indicate outliers with a 0.75 quantile + $1.5 \times$ interquartile range and a 0.25 quantile - $1.5 \times$ interquartile range, respectively.

The POM_{Bed} fraction $< 1\text{ mm}$ consisted of mixed organic debris and clastic sediment, and the coarser fraction $> 1\text{ mm}$ was composed predominantly of organic debris. Only at location $HW_{South-1}$ did the Río San Francisco carry substantial quantities of pebbles in the fraction $> 1\text{ mm}$, while organo-clastic aggregates were more abundant at downstream sites.

The geochemical analysis also revealed substantial differences in the size fractions $> 1\text{ mm}$ and $< 1\text{ mm}$ POM_{Bed} in nearly all samples with sufficient mass for an articulated analysis (Fig. S1). The compositional differences between size fractions, as measured in our limited sample set, lack any discernible systematics, suggesting that variable sourc-

ing affects both size fractions. Variable proportions of woody debris versus leaf fragments, biogeochemical quality, and size distribution indicate significant variability in the sourcing of materials of different sizes at each sampling location of POM_{Bed} even within a single site (Fig. S1b and f). This implies that OM fragments in the Río Bermejo bedload have diverse histories and indicates incomplete mixing both across the channel and along the length of the river, possibly due to highly active channel migration in some parts of the foreland. We did not measure the particle size distributions within individual samples to have sufficient sampling material for geochemical analysis, but we detected a clear reduction in grain size between headwater and downstream locations (Fig. 4).

Geochemically, the similarity of $\text{POM}_{\text{float}}$, leaf litter, soils, sediments, and POM_{Bed} suggests that all of the former can be sources of the sampled POM_{Bed} and no major transformations have occurred during fluvial transit (Fig. 5). Leaf litter and soil inputs from hillslope and riparian areas have potential to be important sources adding to the POM_{Bed} from the headwaters, yet the sampled soils contained little to no coarse POM, suggesting that eroded soil is more likely to become river suspended sediment than POM_{Bed} . Therefore, $\text{POM}_{\text{float}}$ and leaf litter are likely more important contributors to the POM_{Bed} load. Another presumable POM_{Bed} source is abundant woody debris in the catchment; however, this material contains insufficient *n*-alkanes to perform the same analysis. POM_{Bed} CPI_{25-33} values (average: 7.4 ± 3.0 , $n = 39$) were not significantly different from leaf litter (7.4 ± 4.0 , range: 1.0–19.8, $n = 28$) and riverbank sediments (6.5 ± 3.7 , range: 0.3–13.7, $n = 18$). However, on average POM_{Bed} CPI_{25-33} values were significantly higher than in soils (5.9 ± 3.6 , range: 0.2–16.3, $n = 29$) and suspended sediments (5.5 ± 1.0 , range: 1.1–7.8; $n = 41$), indicating a lower maturity of POM_{Bed} . CPI_{25-33} values of $\text{POM}_{\text{float}}$ were substantially higher than values in all sediment samples (15.0 ± 8 , range: 2.4–27.9, $n = 6$), indicating it was, on average, less degraded than other sampled OM.

Before we analyze the details of POM_{Bed} sourcing, we discuss the mechanisms of POM_{Bed} recruitment.

4.1.2 Mechanisms of recruitment and transport of POM_{Bed}

POM_{Bed} is ubiquitous in the bedload of the Río Bermejo throughout the catchment during the high-flow season (December–April), when the South American monsoon drives intense precipitation events throughout the study area. In contrast, we did not recover significant amounts of POM_{Bed} during the low-flow season. The high variability in $\delta^2\text{H}$ values from POM_{Bed} sampled in 2017 and 2020 and the lack of significant amounts of POM_{Bed} during the dry season of 2019 suggest that the processes of recruitment and transport occur quickly, possibly on (sub-)seasonal timescales. The significantly higher CPI_{25-33} values of $\text{POM}_{\text{float}}$ (Fig. 5b) suggest that the degradation of or-

ganic debris occurs after it becomes waterlogged. However, aerobic decomposition seems unlikely during active bedload transport due to the high turbidity and depth of the river water. Instead, fresh plant debris is likely stored intermittently on hillslopes, on floodplains, or in-stream during the low-flow season (May–November), where it can be degraded to various extents and waterlogged. With the onset of strong precipitation and high water levels, it is mobilized by erosion flow, hillslope mass wasting, or lateral channel erosion (e.g., Wohl et al., 2019; Turowski et al., 2016; J. C. Smith et al., 2013; Hilton et al., 2012, 2008; Selva et al., 2007) and subsequently transported as POM_{Bed} (Turowski et al., 2016) during the high-flow season.

In the headwaters, the erosive potential during the high-flow season may exceed the production of organic debris in the riparian corridor on a seasonal timescale, limiting the supply of organic debris to the channel (Hilton et al., 2012; Yager et al., 2012; Garcia et al., 1999) and, consequently, the recruitment of POM_{Bed} . In this case, POM_{Bed} export may peak early in the high-flow season and diminish over the course of the season as the supply of organic debris is progressively reduced with each subsequent rain storm and POM_{Bed} travels steadily downstream, similar to findings of seasonal sourcing of suspended OC at the Río Bermejo (Golombek et al., 2021).

In the lowland floodplain, POM_{Bed} recruitment is also highly seasonal, but the mechanism of recruitment differs from the steep headwater portion of the catchment (Wohl et al., 2019). Lateral channel migration eats into the floodplain forests, mobilizing large volumes of sediment, soil, leaf litter, and standing biomass with each bank failure. Bank erosion is most active at the peak of high-flow season, providing a source of fresh OM to POM_{Bed} and contributing to the poorly mixed nature of POM_{Bed} . However, poorly mixed samples could be expected at high rates of lateral migration from the upstream confluence to ca. 400 km downstream, but enhanced mixing seems more likely in segments with less active migration in the furthest downstream reach of the Río Bermejo. Our results do not indicate enhanced mixing downstream, possibly because of the quick transport timescales compared to the production and recruitment of POM_{Bed} .

Both upland and lowland lateral erosion processes are markedly reduced during the low-flow season, aligning with our observations of ubiquitous POM_{Bed} transport in December–April and negligible POM_{Bed} transport in May–November.

4.2 What are the source areas for recruitment of POM_{Bed} , and does it survive long-range transport?

In the previous section, we concluded that POM_{Bed} is a heterogeneous mixture of OM from various sources in the catchment. In this section, we first aim to determine the stable carbon and hydrogen isotope composition of potential source materials. Subsequently, we apply a model to define the mix-

ing space using source and POM_{Bed} geochemical compositions. In this, our aim is to determine the sources of Río Bermejo POM_{Bed} in order to determine its transformation and fate during long-range transit.

4.2.1 Biomarker stable isotope insights into POM_{Bed} source areas

The stable carbon and hydrogen isotope composition of long-chain *n*-alkanes is used in paleoclimate research to reconstruct continental paleo-vegetation (e.g., Sachse et al., 2012; Huang et al., 2007; Schefuss et al., 2005; Freeman and Colarusso, 2001) or to deduce environmental conditions and potential sources of OM (e.g., Hemingway et al., 2016; Bouchez et al., 2014; Galy et al., 2011; Sachse et al., 2004). Building on these approaches, we use ACL_{25-33} , $n\text{C}_{29}$ $\delta^{13}\text{C}$, and $\delta^2\text{H}$ isotope compositions (Fig. 5) to determine the source areas of POM_{Bed} in the Río Bermejo catchment.

n-Alkane $\delta^{13}\text{C}$ values in plants are controlled by the plant metabolism type, with C_3 plants around -37‰ – -27‰ and C_4 plants around -22‰ – -10‰ (e.g., Garcin et al., 2014; Huang et al., 2007; Freeman and Colarusso, 2001; Collister et al., 1994). Río Bermejo POM_{Bed} $n\text{C}_{29}$ $\delta^{13}\text{C}$ values averaged -32.4 ± 2.9 (range: -36.9‰ – -24.4‰ , $n = 35$, Fig. 5d), reflecting an overall C_3 -dominated plant input (Garcin et al., 2014). Silva et al. (2011) identified a shift towards C_3 vegetation in our study area in the last ~ 3000 years. This imposes an age cap for the organic bedload material, below which our observation of the predominance of fresh to degraded organic material can be accommodated.

There were no distinct differences between the POM_{Bed} $\delta^{13}\text{C}$ values and those for catchment soil ($-34.5\text{‰} \pm 2.2\text{‰}$, range: -40.2‰ – -29.1‰ , $n = 22$), deposited sediment ($-33.7\text{‰} \pm 4.5\text{‰}$, range: -38.0‰ – -18.9‰ , $n = 16$), and floodplain leaf litter ($-33.9\text{‰} \pm 2.2\text{‰}$, range: -39.1‰ – -30.6‰ , $n = 15$), signaling that all these reservoirs are dominated by C_3 inputs (Fig. 5a and c). However, local findings of more positive $\delta^{13}\text{C}$ values and higher ACL_{25-33} (Fig. 7) suggest C_4 plant contributions to POM_{Bed} , possibly from maize cultivation in the HW_{South} catchment area (Powell et al., 2012) and to a lesser extent in the lowland reach near LL_2 (Fig. 1b). Because lateral channel migration rates are low in the downstream reaches of the Bermejo (Repasch et al., 2023, 2020) it is unlikely that local C_4 plants will make it into the bedload in any significant quantities. Finding signatures of C_4 plants in downstream lowland bedload samples provide evidence for long-range transport of POM_{Bed} from the Bermejo headwaters to nearly 1000 km downstream.

$n\text{C}_{29}$ $\delta^2\text{H}$ values can serve as a proxy for the local meteoric water composition taken up by plants, as it is influenced by the water incorporated into plants during photosynthesis (Sachse et al., 2012; Hou et al., 2008; Chikaraishi et al., 2004) and is strongly related to temperature, humidity, rain-

fall amount, moisture source, and elevation (e.g., Walker and Richardson, 1991; Allison et al., 1984; Stewart and Taylor, 1981). In our study area, increasing altitude causes decreasing $\delta^2\text{H}$ values in meteoric water captured in plant tissue: more negative $\delta^2\text{H}$ values corresponded to higher elevations. Nieto-Moreno et al. (2016) measured soil $n\text{C}_{29}$ $\delta^2\text{H}$ values ranging from -150‰ to -110‰ in samples collected along a valley transect ranging from ~ 300 to ~ 4000 m in elevation at a headwater tributary of the Río Bermejo between 22 and 24°S , and the same pattern was described for stream water $\delta^2\text{H}$ values in this region (Rohrmann et al., 2014). Our samples follow these systematics, with $\delta^2\text{H}$ values averaging $-136\text{‰} \pm 15\text{‰}$ (range: -155‰ – -112‰ , $n = 13$) for leaf litter sampled at ~ 270 – 320 m elevation in the Chaco lowland and more negative $\delta^2\text{H}$ values in both leaf litter ($-168\text{‰} \pm 21\text{‰}$, range: -187‰ – -130‰ , $n = 9$) and $\text{POM}_{\text{float}}$ ($-160\text{‰} \pm 7\text{‰}$, range: -171‰ – -153‰ , $n = 5$) collected upstream of the confluence.

^2H depletion correlates significantly with increasing elevation in floodplain and headwater leaf litter samples (Fig. 6, $y = -640 - 6.4x$, $R^2 = 0.557$, $p < 0.01$). This is true also for the $\text{POM}_{\text{float}}$ samples but not significantly ($y = -3606 - 30x$, $R^2 = 0.14$, $p > 0.05$). The sampling transect for $\text{POM}_{\text{float}}$ covers a rapid westward precipitation decline, where samples from > 1000 m a.s.l. are likely sourced from arid areas, whereas the samples from lower elevations receive orographic precipitation, suggesting that the gradient in precipitation amount may cause the observed ^2H depletion and the worse fit in $\text{POM}_{\text{float}}$ samples.

Nevertheless, the elevation-dependent $\delta^2\text{H}$ composition is caused by a precipitation-dependent change in $\delta^2\text{H}$ values of the areas covered by our study, as shown by Nieto-Moreno et al. (2016) and Rohrmann et al. (2014): upland areas are depleted in ^2H compared to the Río Bermejo lowland, where convective precipitation is the main source of moisture (Rohrmann et al., 2014). We take advantage of this elevation-dependent trend in source POM $\delta^2\text{H}$ values to identify source elevations of the POM_{Bed} samples, where more negative $\delta^2\text{H}$ values indicate a higher-elevation origin, and less negative $\delta^2\text{H}$ values signal a low-elevation floodplain origin. POM_{Bed} samples do not show such a correlation of sampling elevation with $\delta^2\text{H}$ values, and we suggest this is due to transport between production and sampling of this material.

4.2.2 Mixing model analysis

We defined three potential POM_{Bed} sources from coarse organic debris we sampled at distinct elevations in the catchment: floodplain leaf litter (< 320 m), headwater leaf litter (320 – 1000 m), and headwater $\text{POM}_{\text{float}}$ (> 320 m). Significant end-member unmixing of the respective sources to the mixed POM_{Bed} signal is not expedient using the geochemical proxies applied in this study. Instead, we aim to understand the mixing range of the widely spread POM_{Bed} . We determine the range of a possible POM_{Bed} mixing signal of

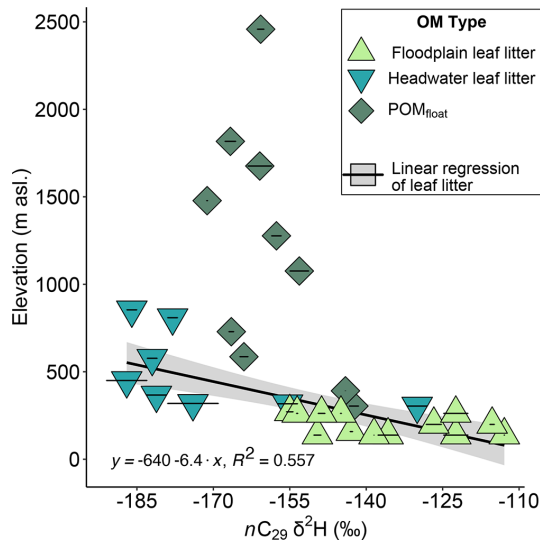


Figure 6. Sampling elevation and $nC_{29} \delta^2H$ values of floodplain and headwater leaf litter, as well as POM_{float} . Colors represent the organic matter type; symbols represent the catchment source area. The linear regression was done using floodplain and headwater leaf litter data. Linear regression of POM_{float} samples is not shown and was not significant. Measurement uncertainty is plotted inside the symbol.

the sources within the geochemical parameters and, in addition, determine potential missing POM_{Bed} sources. We use a mixing space model developed by J. A. Smith et al. (2013). In short, the model uses Monte Carlo simulations to iterate mixing spaces (“convex hulls”), outlining the probability that observed POM_{Bed} sample compositions can be explained by a mixing model of the proposed sources. The model utilizes resampled source averages and their standard deviations and considers the distribution of the mix data (POM_{Bed} data) within a pre-defined mixing space.

For our purpose, we assume uniform source mixing of the POM_{Bed} samples without fractionation from the source composition of POM_{float} , floodplain, and headwater leaf litter δ^2H/ACL_{25-33} and $\delta^2H/\delta^{13}C$ to POM_{Bed} . We use minimum and maximum boundary conditions based on our source data to define the extent of the initial mixing space: 25 to 35 for the ACL_{25-33} , -190‰ and -110‰ for δ^2H values, and -40‰ and -20‰ for $\delta^{13}C$ values. The initial mixing space is iteratively adapted over 2000 iterations using source data average and standard deviation, resampled from a normal distribution. Through each iteration, a point-in-polygon algorithm tests if the mixed POM_{Bed} data remain within the iteratively adapted mixing space. This ensures an “optimization” of the mixing space according to our POM_{Bed} data, permitting us to evaluate if the actual POM_{Bed} sources are not fully represented by our included sources. The point-in-polygon algorithm is applied to a testing grid within the mixing space. With a grid resolution of 500‰^2 , the point-in-polygon algorithm is tested on 500×500 values per iteration within the

mixing region. Simultaneously, the area of the mixing space is assessed, and the variance between all previous iterations is calculated. The stabilized variance value, then, represents the optimized mixing space area for the available source data and the mixed POM_{Bed} data.

The variance of the convex hull area stabilized after ~ 1000 iterations for the δ^2H/ACL_{25-33} model at a variance of 40‰^2 and after ~ 1000 iterations for $\delta^2H/\delta^{13}C$ at a variance of 60‰^2 . The resulting mixing regions were not sensitive to variations of the boundary conditions. The results are plotted as derived mixing regions, with different levels of confidence representing the likelihood with which the observed data can result from mixing of the source data (Fig. 7).

4.2.3 Mixing model insights into POM_{Bed} source areas

We proceed to use floodplain leaf litter, headwater leaf litter, and headwater POM_{float} $ACL_{25-33}/nC_{29} \delta^2H$ and $nC_{29} \delta^{13}C/nC_{29} \delta^2H$ values as potential sources to create mixing regions for our POM_{Bed} samples (Fig. 7a and b). Half of the samples follow the $\delta^2H/\delta^{13}C$ compositional trend of leaf litter ($y = -234.8x + 10.8$, $R^2 = 0.94$), with $nC_{29} \delta^2H$ values ranging from -174‰ – -112‰ and $\delta^{13}C$ values ranging from -39.0‰ – -30.0‰ (Fig. 7c). This indicates that locally supplied floodplain leaf litter is an important source to the sampled POM_{Bed} , as already suggested earlier. In these samples, this lowland-derived plant material dominates over any existing bedload sourced from upstream areas.

A total of 20% of the POM_{Bed} samples fall within the region of the $nC_{29} \delta^{13}C/nC_{29} \delta^2H$ mixing space defined by headwater sources. This suggests input from at least one high-elevation upland source. Evidence for this high-elevation OM source in lowland POM_{Bed} samples confirms that mountain-derived OM can survive long-range bedload transport in the Río Bermejo.

One-third of the POM_{Bed} samples fall outside the 95% confidence interval of the $\delta^2H/\delta^{13}C$ mixing space, while some POM_{Bed} samples collected from both the headwaters and the lowland are not within the wider mixing space constrained by δ^2H/ACL_{25-33} (Fig. 7c and d). These samples have $nC_{29} \delta^2H$ values ranging from -125‰ – -150‰ and $nC_{29} \delta^{13}C$ values ranging from -27‰ – -33‰ (see labeled POM_{Bed} samples in Fig. 7). This suggests input from at least one additional, herein unconstrained, source, and the comparably heavy $\delta^{13}C$ values suggest this could contain C_4 plant contributions. C_4 plants grow only sparsely in the catchment (Fig. 1b) and mostly on agricultural land in HW_{South} . We suggest that the missing source in our samples is farmland OM, which would indicate that the POM_{Bed} carbon flux can be directly influenced by anthropogenic land use.

Sediment load data from gauging stations on the upper Río Bermejo and Río San Francisco indicate that HW_{North} contributes 6 times more suspended sediment load to the lowland Río Bermejo than HW_{South} (Repasch et al., 2020). There is

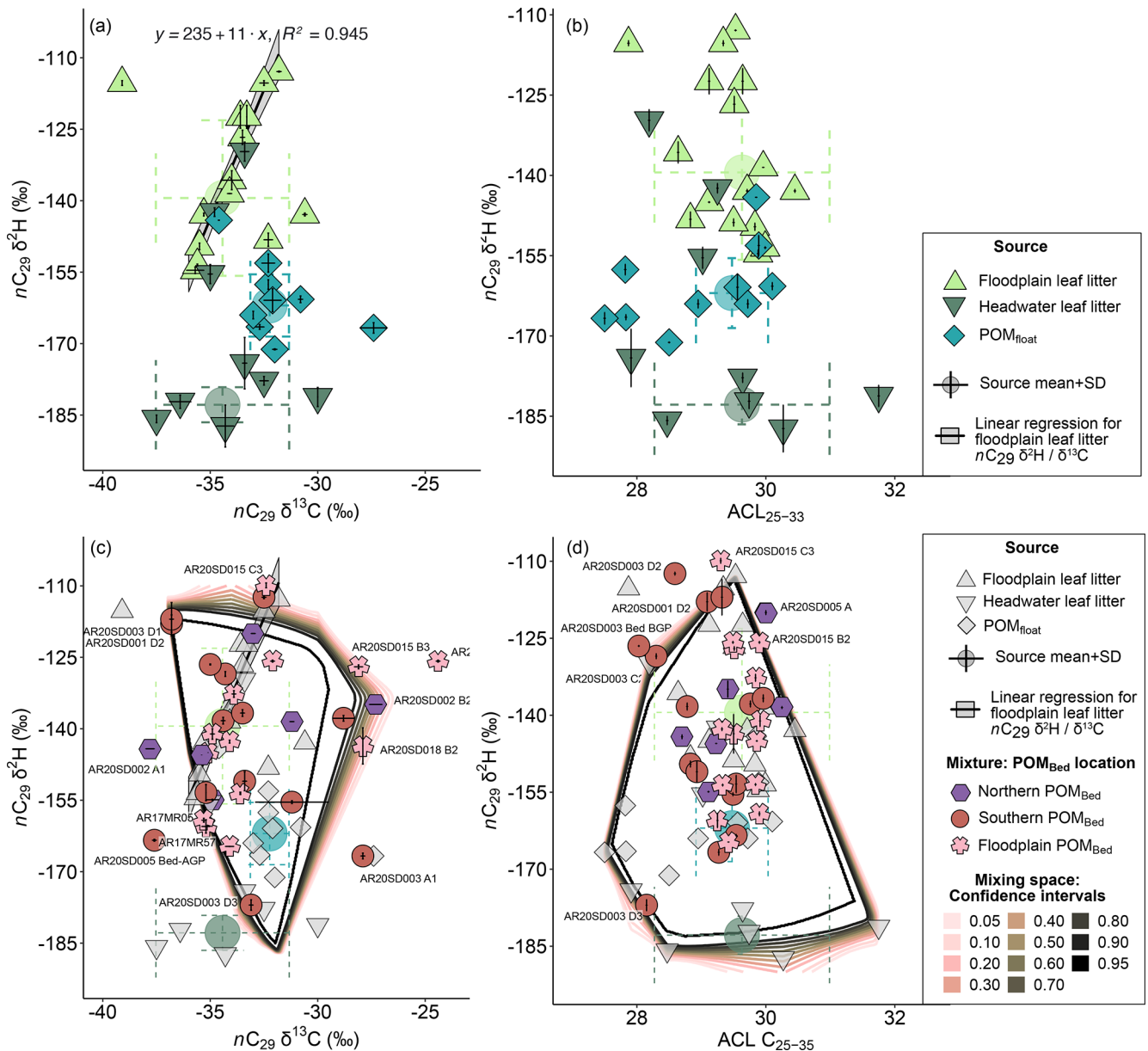


Figure 7. Upper panels (a, b): headwater and floodplain leaf litter and POM_{float} samples with the average \pm standard deviation depicted as potential POM_{Bed} sources using (a) $nC_{29} \delta^2H$ versus $nC_{29} \delta^{13}C$ and (b) $nC_{29} \delta^2H$ versus ACL_{25-33} . Lower panels (c, d): grayed-out area symbols and colored averages correspond to the OM sources from panels (a) and (b). Colored symbols are POM_{Bed} samples from headwaters and floodplains for (a) $nC_{29} \delta^2H$ versus $nC_{29} \delta^{13}C$ and (b) $nC_{29} \delta^2H$ versus ACL_{25-33} . Colored lines are probability contours of the simulated mixing area (J. A. Smith et al., 2013) using the organic matter source. The outermost contour represents the 5% confidence level and the innermost contour the 95% confidence level. Labeled POM_{Bed} samples are those that fall outside the mixing area and the source area of both plots. Uncertainty is plotted inside the symbol. Linear regression in panels (a) and (c) was conducted using lowland leaf litter data.

a north-to-south rainfall gradient with almost 3 times more precipitation in HW_{North} (Fig. 1c, Hijmans et al., 2005), indicating higher erosion potential and possibly causing more recruitment of organic bedload from this area (Galy et al., 2015). This suggests that the HW_{North} source area should dominate organic input from the headwaters. However, this

cannot be constrained with the geochemical proxies adopted in this study.

4.3 Long-range transport of POM_{Bed}

Recent studies show that fresh, coarse organic debris can generally be found near the riverbed (Repasch et al., 2022;

Schwab et al., 2022; Feng et al., 2016), but the implications of this transport for the OC cycle are underconstrained. Using our new understanding of the POM_{Bed} source areas and the evolution downstream, we now consider the fate of POM_{Bed} during long-range fluvial transport through the Río Bermejo lowland river system.

The proportion of POM transported at the bed versus in suspension is a function of particle size, density, and shape, the recalcitrance of the POM, the river's turbulence, sediment load, the flow close to the bed (Turowski et al., 2016; Nichols et al., 2000), and secondary flow motions (Schwab et al., 2022). We assume that POM_{Bed} moves as clastic bedload, with a pace of about 0.7 times the depth-averaged flow velocity (Chatanantavet et al., 2013), which is around 0.46 ms^{-1} (average of positive flow velocities, Dosch et al., 2023) at both the Bermejo–San Francisco confluence and downstream locations. At this velocity, a POM_{Bed} parcel could be transported 1300 km through the Río Bermejo floodplain in ~ 45 d. Moreover, slightly higher CPI_{25–33} values at downstream sites (average: 8.2 ± 3.0 , range 4.9–15.2, $n = 14$, Fig. 5) versus upstream (average: 6.9 ± 3.0 , range 0.1–11.7, $n = 25$, Fig. 5) suggest there is no systematic, progressive degradation of POM_{Bed} during long-range fluvial transport, likely because transport timescales are too short to produce significant chemical degradation. This demonstrates that POM_{Bed} can travel from the Andean headwaters into the Río Paraguay within one single high-flow season in the Río Bermejo. It explains the absence of POM_{Bed} during the low-flow season when little OM is likely to come in from outside the river channel. Moreover, it elucidates the occurrence of coarse organic debris in turbidity currents and turbidite deposits, where it is buried under finer clastic sediments (Hage et al., 2020; Lee et al., 2019; McArthur et al., 2016; Sparkes et al., 2015).

Once entrained, POM_{Bed} likely moves as a semi-separate layer in deep and fast-flowing parts of the channel cross-section where bed shear stress is greatest. Without substantial mixing, parcels of POM_{Bed} may shuffle downstream due to discrete erosion events at high flow and deposition at low flow. Episodic flushing events of the channel can transport parcels efficiently (Heijnen et al., 2022) and facilitate waterlogging of the organic debris (West et al., 2011). Waterlogged coarse organic debris is not prone to spilling onto the riverbank or across levees into adjacent flood basins and can progress downstream. Thus, the downstream advection of POM_{Bed} in the Río Bermejo may be sustained by seasonal high flow driven by monsoonal rainfall and quasi-uninterrupted by intermittent deposition. The helical flow induced by the constant meandering of the lower Río Bermejo could augment this process (Schwab et al., 2022). As such, significant amounts of OM could be efficiently transported with bedload through large drainage basins from mountainous uplands to marine basins on sub-seasonal timescales.

Mechanical comminution of POM_{Bed} during long-range transport

Despite evidence for survival during long-range fluvial transport, we might expect that the physical interaction between bedload OM and clastic particles can cause comminution of organic particles (Dosch et al., 2021; Scheingross et al., 2019; Turowski et al., 2016; Hilton et al., 2012; Attal and Lavé, 2009; Nichols et al., 2000) and that comminuted POM_{Bed} transfers into the river suspended load. The observed decrease in POM_{Bed} sample size with increasing distance downstream from the confluence suggests a progressive loss of POM_{Bed} (Fig. 4d), despite the input of OM from lateral erosion of the lowland floodplain. The similarity between *n*-alkane $\delta^{13}\text{C}$, $\delta^2\text{H}$, and ACL_{25–33} values of the Río Bermejo suspended sediment and POM_{Bed} (Fig. 5) implies that the two fractions share an origin. River suspended sediment samples yielded similar CPI_{25–33} values, on average 5.5 ± 1.0 (range: 1.1–7.8; $n = 41$), but with less variability and values only as high as 7.8, suggesting advanced mixing and maturity compared to POM_{Bed} (average: 29.6 ± 0.9 , range 27.4–31.6, $n = 39$).

The particle size distributions of POM_{Bed} samples from downstream locations were considerably finer than samples from the confluence, even if the recovered sample sizes did not permit separation of aliquots for grain size measurements. As flow velocities increase, POM_{Bed} particles may increasingly transfer into suspension rather than traveling at the riverbed (Turowski et al., 2016). This transition is smooth, and POM_{Bed} may move in saltation at the transition between the two transport modes (e.g., Turowski et al., 2016; Nichols et al., 2000). However, flow velocities along the Río Bermejo main stem show no significant variability; therefore, transfer from POM_{Bed} to the suspended load is more likely to result from the comminution of coarse particles rather than changes in river hydrodynamics. To our knowledge, there are no experimental or field data showing comminution of particulate organic matter. However, Merten et al. (2013) suggested that physical breakage of large woody debris in streams is likely dominantly controlled by the structural properties and the in-stream position of the organic matter as opposed to hydraulic and geomorphic variables, concurring with our interpretation. Further research is needed to determine the scope and controlling factors of physical decay of coarse organic matter in the water column.

5 Synthesis: bedload carbon fluxes at the Río Bermejo

We close with a provisional examination of the organic carbon flux associated with bedload transport, its relation to suspended transport, and its role in the terrestrial carbon cycle. We extrapolated our local, high-flow season point measurements of POM_{Bed} across the respective river transects, ignoring any OM particles < 1 mm in near-bed transport, and used

a simple upscaling approach to estimate the flux of organic carbon with bedload POC_{Bed} (in tC yr^{-1}).

$$\text{POC}_{\text{Bed}} = \frac{\sum \text{POM}_{\text{Bed}} \times \frac{\text{Transect width} \times 0.5}{\text{Funnel width}} \times 0.58}{t_{\text{sampling}}} \times t_{\text{transport}} \quad (3)$$

We sum the sampled POM_{Bed} ($\text{POM}_{\text{Bed}} > 1 \text{ mm}$, in $\text{mass} \times \text{min}^{-1}$), apply the van Bemmelen factor of 0.58 to represent the carbon content in (soil) organic matter (Allison, 1965), and divide by the sampling time t_{sampling} (in min) along each transect using the respective standard deviation of POM_{Bed} to define an upper and lower boundary of the estimated bedload carbon flux. To do this, we extrapolated the samples obtained with a funnel opening of 0.08 m to the central 50 % of the river channel (transect width $\times 0.5$, in m^2), where it is assumed that POM_{Bed} transport is concentrated. Since we did not capture significant amounts of POM_{Bed} during the dry season, we assumed that POM_{Bed} transport only occurs during the 6 months of the high-flow season ($t_{\text{transport}} = 182.5 \text{ d}$). This approach allowed us to estimate POC_{Bed} without using near-bed velocities that were not available for all locations.

HW_{North} and HW_{South} both show an increase in the POM_{Bed} flux from the upper headwater locations ($\text{HW}_{\text{North-2}}$ and $\text{HW}_{\text{South-2}}$, respectively) to the lower headwater locations ($\text{HW}_{\text{North-1}}$ and $\text{HW}_{\text{South-1}}$, respectively), demonstrating the possibility of fast recruitment of POM_{Bed} in short distances. To determine changes in mass flux from the mountain front to the downstream reaches, we compare the combined headwater fluxes to those estimated at downstream sampling sites. The fluxes of POM_{Bed} at the upper Río Bermejo at $\text{HW}_{\text{North-1}}$ and Río San Francisco at $\text{HW}_{\text{South-1}}$ define the flux into the low-gradient portion of the river. We estimate the POM_{Bed} fluxes from HW_{South} and HW_{North} at 926–1138 tC yr^{-1} and 112–188 tC yr^{-1} , respectively, for a total of 1038–1326 tC yr^{-1} exported from the headwaters to the lowland reach (Fig. 8, Table 2). Downstream at LL_1 , we calculate a POM_{Bed} flux of 155–351 tC yr^{-1} , while at LL_2 we estimate 19–27 tC yr^{-1} .

It is difficult to reconcile the minimum 66 % loss of C in bedload between the Bermejo–San Francisco confluence and LL_1 (865 km transport distance) with the subsequent large apparent 10-fold reduction of the bedload C flux from LL_1 to LL_2 over a transport distance of only $\sim 220 \text{ km}$. The downstream increase in POM_{Bed} aggregates that dissociated into $\text{POM}_{\text{Bed}} < 1 \text{ mm}$ could cause an underestimation of the $\text{POM}_{\text{Bed}} > 1 \text{ mm}$ flux at LL_2 . The discrepancy may further be due to sampling bias (Turowski et al., 2013), bedload flux variability due to bedforms, the formation of OM waves at the channel bed, interspersed with relatively barren intervals (Heijnen et al., 2022), strongly sustained discharge (e.g., Rickenmann, 2018; Turowski et al., 2016; Reid et al., 1998), and channel geometry (Fogel and Lininger, 2023). Bedload sampling, particularly using Helley–Smith samplers, can be prone to high variability, and we suggest that our estimates are an order-of-magnitude approximation (Bunte et al., 2008)

that likely underestimates the maximum POM_{Bed} transport rate. This could also cause the flux rates of HW_{South} that exceed the fluxes at HW_{North} , despite the higher erosive potential at HW_{North} . More agricultural activities in HW_{South} could also enhance surface erosion and with that OM input locally. Our approach assumes that the dimension of the POM_{Bed} layer and its individual particles are within the constraints of the funnel height of the sampler and that the samples and sampling points across each transect represent the cross-section of the channel. A larger sample size and sampled surface area, longer sampling times, and better understanding of distribution and dynamics of the POM_{Bed} layer could greatly enhance the accuracy of the sample set and flux estimates. Despite these uncertainties, this is the first estimate of its kind and shows that river POM fluxes may be underestimated without considering the bedload OM flux.

The inferred POM_{Bed} grain size reduction during transport, similar to clastic sediment (Attal and Lavé, 2009), contributes to the overall suspended sediment yield of the river. The total suspended organic carbon flux is $\sim 1.85 \times 10^5 \text{ tC yr}^{-1}$ at the Bermejo–San Francisco confluence (Repasch et al., 2021), suggesting that the estimated POM_{Bed} carbon flux near the confluence is less than 1 % of the total carbon load. The Río Bermejo exports $\sim 2.24 \times 10^5 \text{ tC yr}^{-1}$ in suspension downstream to the Río Paraguay, implying that about $0.39 \times 10^5 \text{ tC yr}^{-1}$ of suspended organic carbon is delivered to the lowland channel by lateral erosion (Repasch et al., 2021). If we take the downstream estimates of bedload C flux at face value and assume this loss transfers to the suspended load, a mass balance suggests that less than 1 % of the suspended load gain between the confluence and LL_1 and LL_2 could be due to grain size reduction of the coarse organic load. While our bedload carbon flux estimates are tentative, it is clear that this eye-catching mode of organic carbon transfer is small in comparison with the fluvial export of organic carbon in the suspended load of the Río Bermejo.

However, the Río Bermejo's suspended sediment yield is exceptionally high (Sambrook Smith et al., 2016). Assuming the loss between the $\text{HW}_{\text{South-1}} + \text{HW}_{\text{North-1}}$ and LL_1 as well as LL_2 transfers completely to the suspended load, 79 % and 98 %, respectively, of POM_{Bed} would transfer into suspension while simultaneously recruiting additional bedload from the floodplain. POM_{Bed} in rivers and sedimentary deposits could contribute substantially to the overall flux in river systems with lower suspended sediment yield and where bedload dominates the fluvial sediment flux (Turowski et al., 2016) or in highly erosive headwater streams with short transport distances from recruitment to subsequent deposition and burial (Blair and Aller, 2012; Hilton et al., 2011).

This coarse particulate OM may also have a higher probability of preservation and rapid burial in depositional basins, as its particle settling velocity is higher than smaller particles and may be less prone to resuspension and oxidation. Future work should aim to enhance our understanding of the signifi-

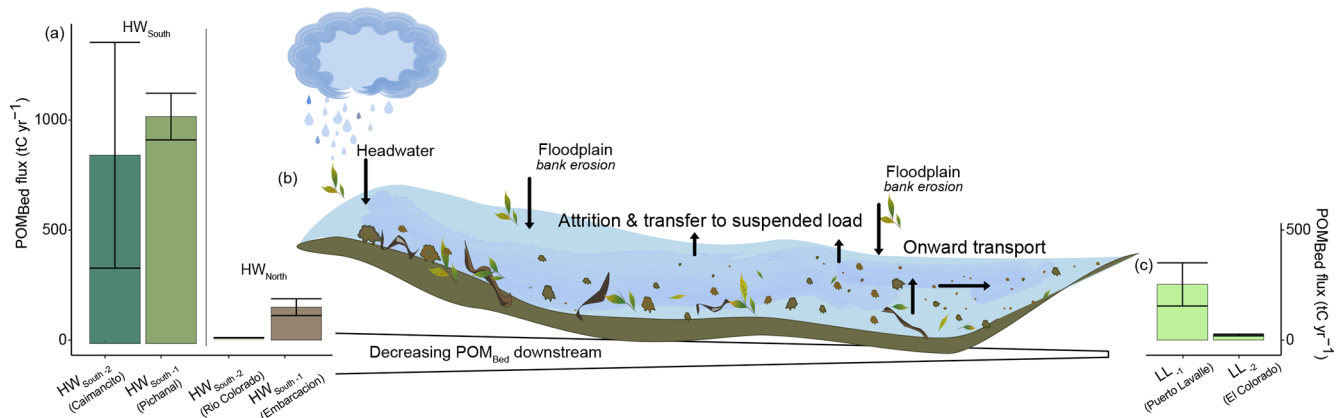


Figure 8. (a) Bar plot showing the order-of-magnitude estimates (\pm standard deviation) of the POM_{Bed} flux (tC yr^{-1}) at HW_{South} and HW_{North} . (b) Illustration of the source areas, transport, and fate of POM_{Bed} at the Río Bermejo from upstream recruitment downstream: sourcing from the headwater and the floodplain during wet-season erosion, partial attrition and transfer to suspended load causing a net decrease in POM_{Bed} , and onward transport of the remaining POM_{Bed} leading to (c) order-of-magnitude estimates of the lowland POM_{Bed} flux (tC yr^{-1}).

Table 2. Bedload sampling locations and yields from the field campaign in 2020, as well as the estimated flux of particulate organic carbon on the riverbed.

Location name	Sampling time t_{sampling} (min)	Total sum bedload (g)	Total sum POM_{Bed} > 1 mm (g)	Full transect width (m)	Average near-bed flow velocity \pm standard deviation ^a (m s^{-2})	POC_{Bed} flux \pm standard deviation ^b (tC yr^{-1})
$\text{HW}_{\text{South-2}}$ (Caimancito)	2	588	22	80	NA	855 ± 513
$\text{HW}_{\text{North-1}}$ (Embarcación)	4	2589	5	169	0.29 ± 0.3	150 ± 38
$\text{HW}_{\text{South-1}}$ (Pichanal)	11	7283	66	183	0.49 ± 0.3	1032 ± 106
$\text{HW}_{\text{North-2}}$ (Río Colorado)	4	955	3	35	NA	11 ± 1
LL-1 (Puerto Lavalley)	7	617	9	215	-0.19 ± 0.4	253 ± 98
LL-2 (El Colorado)	5	617	1	90	0.27 ± 0.6	23 ± 4

NA: not available. ^a Measured using ADCP. ^b Calculated using Eq. (3).

importance of POM_{Bed} export and burial over varying transport length scales.

6 Conclusion

In this study, we investigated the occurrence, recruitment mechanisms, source areas, and survival of POM_{Bed} during long-range transport to understand the implications for the terrestrial organic carbon cycle. We found the persistent occurrence of POM_{Bed} along a 1300 km section of the Río

Bermejo in northern Argentina from the headwaters to its confluence with the Río Paraguay.

Our results provide evidence that the POM_{Bed} originates from erosion of fresh, terrestrial organic debris from the local floodplain, as well as distal headwater sources, and is composed of a heterogeneous mix from catchment-wide sources, dominated by C_3 plant input, and local C_4 point sources. POM_{Bed} can remain geochemically unaltered over long fluvial transport distances due to fast transport. The high geochemical variability within and between the bedload sampling transects (Fig. S2) does not allow a quantitative un-

mixing of POM_{Bed} sources; however, this variability indicates that POM_{Bed} may travel in parcels, each representing an erosive event that delivered fresh OM to the river, where it was subsequently waterlogged and translocated to the channel bed. Our data suggest coherent and continuous transport of individual OM parcels at the riverbed such that POM_{Bed} is never fully mixed longitudinally in a river system. Although POM_{Bed} appears to survive long-range fluvial transport, it can mechanically break down during transport, contributing to the overall suspended sediment load of the river. After physical breakdown, the fate of POM_{Bed} does not lay exclusively in the suspended fraction. The geochemical proxies for the Río Bermejo soil and bank sediment suggest it can also be stored on floodplains and undergo partial mineralization. Changes in hydraulic settings can lead to particle settling, and high suspended sediment yields enhance the burial efficiency and promote drawdown of atmospheric CO_2 over longer timescales.

The decreasing POM_{Bed} flux downstream also indicates that the loss of POM_{Bed} exceeds the recruitment from the floodplain and therefore that local ecosystem productivity is likely not the main factor controlling POM_{Bed} genesis at the Río Bermejo. Rather, the main control is likely to be the pre-conditioning of OM such that it can rapidly absorb water, increasing its density and its settling velocity, allowing it to sink (Hoover et al., 2010). Overland flow is also necessary to facilitate OM erosion and transport to the active channel, and sufficient river flow velocity is required to maintain transport at the bed (Galy et al., 2015). Likewise, the ratio of POM_{Bed} export and potential burial versus abrasion and transport as suspended sediment likely depends on plant type, climate, river morphology, hydrodynamics, and transit time (Hoover et al., 2010).

We found that transport of POM_{Bed} is not a major contributor to carbon burial on short timescales at the Río Bermejo, but ongoing floodplain recruitment contributes to the genesis of POM_{Bed} , and fluvial transport could export POM_{Bed} from the headwaters to the ocean on short timescales, representing a hitherto under-investigated mechanism for fluvial organic carbon export and burial. Bedload transport can convey OM to downstream basins with subsequent burial over millennial timescales; however, this is possibly more significant for shorter transport distances. The abundance and magnitude of bedload is in general highly variable and notoriously difficult to measure, and it remains challenging to quantify the total amount of POM_{Bed} due to stochasticity of bedload transport and the heterogeneity of POM_{Bed} abundance. Our approach is a first step to evaluate the origin and fate of POM_{Bed} during long-range fluvial transport in a natural setting. Further experimental and field studies are necessary to improve our understanding of the fraction of POM transported as bed material versus in the water column.

Code and data availability. Additional data referred to in the main text, data tables, and model code are available in the Supplement: <https://doi.org/10.5880/GFZ.4.6.2023.005> (Dosch et al., 2023).

Supplement. The supplement related to this article is available online at: <https://doi.org/10.5194/esurf-12-907-2024-supplement>.

Author contributions. SD prepared the manuscript with contributions from all co-authors. SD, NH, MR, JS, JMT, and DS conceptualized the manuscript. Visualization and formal analysis were conducted by SD. SD, NH, MR, ST, DS, JMT, and OR developed the methodology and performed the investigation process. NH and DS acquired the funding and administrated the project.

Competing interests. At least one of the (co-)authors is a member of the editorial board of *Earth Surface Dynamics*. The peer-review process was guided by an independent editor, and the authors also have no other competing interests to declare.

Disclaimer. Publisher's note: Copernicus Publications remains neutral with regard to jurisdictional claims made in the text, published maps, institutional affiliations, or any other geographical representation in this paper. While Copernicus Publications makes every effort to include appropriate place names, the final responsibility lies with the authors.

Acknowledgements. We thank Manfred Strecker for securing the funding for this research. We thank Yani Roja and Daniel Herrmann for invaluable support during work, Emiliy Ikawy for her help with lab work, Christoff Andermann for his guidance with the ADCP, and Gunnar Pruß for technical and lab support.

Financial support. This research was funded by the Deutsche Forschungsgemeinschaft (DFG) and the Federal State of Brandenburg under the auspices of the International Research Training Group IGK2018 “SuRfAce processes, TEctonics and Georesources: The Andean foreland basin of Argentina” (STRATEGY), DFG grant STR 373/34-1 to Manfred Strecker.

The article processing charges for this open-access publication were covered by the Helmholtz Centre Potsdam – GFZ German Research Centre for Geosciences.

Review statement. This paper was edited by Edward Tipper and reviewed by Kasey Clark and J. Jotautas Baronas.

References

- Allen, G. P., Laurier, D., and Thouvenin, J.: Étude sédimentologique du delta de la Mahakam, Compagnie Française des Pétroles, Notes et Mémoires, 1–156, 1979.
- Allen, J. R. L.: Current Ripples. Their relation to patterns of water and sediment motion, *Geol. Mag.*, 106, 614–614, <https://doi.org/10.1017/S001675680005946X>, 1968.
- Aller, R. C.: Mobile deltaic and continental shelf muds as suboxic, fluidized bed reactors, *Mar. Chem.*, 61, 143–155, [https://doi.org/10.1016/S0304-4203\(98\)00024-3](https://doi.org/10.1016/S0304-4203(98)00024-3), 1998.
- Allison, G. B., Barnes, C. J., Hughes, M. W., and Leaney, F. W. J.: Effect of climate and vegetation on oxygen-18 and deuterium profiles in soils, IAEA – International Atomic Energy Agency, 15, 105–123, 1984.
- Allison, L. E.: Organic Carbon, in: *Methods of Soil Analysis*, Wiley, 1367–1378, <https://doi.org/10.2134/agronmonogr9.2.c39>, 1965.
- Attal, M. and Lavé, J.: Pebble abrasion during fluvial transport: Experimental results and implications for the evolution of the sediment load along rivers, *J. Geophys. Res.*, 114, F04023, <https://doi.org/10.1029/2009jf001328>, 2009.
- Battin, T. J., Luysaert, S., Kaplan, L. A., Aufdenkampe, A. K., Richter, A., and Tranvik, L. J.: The boundless carbon cycle, *Nat. Geosci.*, 2, 598–600, <https://doi.org/10.1038/ngeo618>, 2009.
- Berner, R. A.: Burial of organic carbon and pyrite sulfur in the modern ocean – Its geochemical and environmental significance, *Am. J. Sci.*, 282, 451–473, <https://doi.org/10.2475/ajs.282.4.451>, 1982.
- Blair, N. E. and Aller, R. C.: The fate of terrestrial organic carbon in the marine environment, *Annu. Rev. Mar. Sci.*, 4, 401–423, <https://doi.org/10.1146/annurev-marine-120709-142717>, 2012.
- Blattmann, T. M., Liu, Z., Zhang, Y., Zhao, Y., Haghpor, N., Montluçon, D. B., Plötze, M., and Eglinton, T. I.: Mineralogical control on the fate of continentally derived organic matter in the ocean, *Science*, 366, 742–745, <https://doi.org/10.1126/science.aax5345>, 2019.
- Bouchez, J., Galy, V., Hilton, R. G., Gaillardet, J., Moreira-Turcq, P., Pérez, M. A., France-Lanord, C., and Maurice, L.: Source, transport and fluxes of Amazon River particulate organic carbon: Insights from river sediment depth-profiles, *Geochim. Cosmochim. Ac.*, 133, 280–298, <https://doi.org/10.1016/j.gca.2014.02.032>, 2014.
- Bray, E. E. and Evans, E. D.: Distribution of n-pamLEns as a clue to recognition of source beds, *Geochim. Cosmochim. Ac.*, 22, 2–15, [https://doi.org/10.1016/0016-7037\(61\)90069-2](https://doi.org/10.1016/0016-7037(61)90069-2), 1961.
- Bunte, K., Abt, S. R., Potyondy, J. P., and Swingle, K. W.: A Comparison of Coarse Bedload Transport Measured with Bedload Traps and Helley-Smith Samplers, *Geodin. Acta*, 21, 53–66, <https://doi.org/10.3166/ga.21.53-66>, 2008.
- Bunte, K., Swingle, K. W., Turowski, J. M., Abt, S. R., and Cenderelli, D. A. A.: Measurements of coarse particulate organic matter transport in steep mountain streams and estimates of decadal CPOM exports, *J. Hydrol.*, 539, 162–176, <https://doi.org/10.1016/j.jhydrol.2016.05.022>, 2016.
- Canuel, E. A. and Hardison, A. K.: Sources, Ages, and Alteration of Organic Matter in Estuaries, *Annu. Rev. Mar. Sci.*, 8, 409–434, <https://doi.org/10.1146/annurev-marine-122414-034058>, 2016.
- Chatanantavet, P., Whipple, K. X., Adams, M. A., and Lamb, M. P.: Experimental study on coarse grain saltation dynamics in bedrock channels, *J. Geophys. Res.-Earth*, 118, 1161–1176, <https://doi.org/10.1002/jgrf.20053>, 2013.
- Chikaraishi, Y., Naraoka, H., and Poulson, S. R.: Hydrogen and carbon isotopic fractionations of lipid biosynthesis among terrestrial (C3, C4 and CAM) and aquatic plants, *Phytochemistry*, 65, 1369–1381, <https://doi.org/10.1016/j.phytochem.2004.03.036>, 2004.
- Collister, J. W., Rieley, G., Stern, B., Eglinton, G., and Fry, B.: Compound-specific $\delta^{13}\text{C}$ analyses of leaf lipids from plants with differing carbon dioxide metabolisms, *Org. Geochem.*, 21, 619–627, [https://doi.org/10.1016/0146-6380\(94\)90008-6](https://doi.org/10.1016/0146-6380(94)90008-6), 1994.
- Cranwell, P. A.: Chain-length distribution of *n*-alkanes from lake sediments in relation to post-glacial environmental change, *Freshwater Biol.*, 2, 259–265, 1972.
- Dellinger, M., Hilton, R. G., Baronas, J. J., Torres, M. A., Burt, E. I., Clark, K. E., Galy, V., Ccahuana Quispe, A. J., and West, A. J.: High Rates of Rock Organic Carbon Oxidation Sustained as Andean Sediment Transits the Amazon Foreland-Floodplain, *P. Natl. Acad. Sci. USA*, 120, e2306343120, <https://doi.org/10.1073/pnas.2306343120>, 2023.
- Dosch, S., Hovius, N., Repasch, M., Scheingross, J., Turowski, J., and Sachse, D.: Terrestrial biospheric carbon export from rivers by bedload transport, EGU General Assembly 2021, online, 19–30 Apr 2021, <https://doi.org/10.5194/egusphere-egu21-10684>, 2021.
- Dosch, S., Hovius, N., Repasch, M., Scheingross, J., Tofelde, S., Turowski, J., Rach, O., and Sachse, D.: Sourcing and Long-Range Transport of Particulate Organic Matter in River Bedload: Rio Bermejo, Argentina, GFZ Data Services [data set], <https://doi.org/10.5880/GFZ.4.6.2023.005>, 2023.
- Eglinton, G. and Hamilton, R. J.: Leaf Epicuticular Waxes, *Science*, 156, 1322–1335, <https://doi.org/10.1126/science.156.3780.1322>, 1967.
- Einstein, H. A., Anderson, A. G., and Johnson, J. W.: A distinction between bed-load and suspended load in natural streams, *Eos, Transactions American Geophysical Union*, 21, 628–633, <https://doi.org/10.1029/TR021i002p00628>, 1940.
- Feng, X., Feakins, S. J., Liu, Z., Ponton, C., Wang, R. Z., Karkabi, E., Galy, V., Berelson, W. M., Nottingham, A. T., Meir, P., and West, A. J.: Source to sink: Evolution of lignin composition in the Madre de Dios River system with connection to the Amazon basin and offshore, *J. Geophys. Res.-Biogeol.*, 121, 1316–1338, <https://doi.org/10.1002/2016jg003323>, 2016.
- Fogel, C. B. and Lininger, K. B.: Geomorphic complexity influences coarse particulate organic matter transport and storage in headwater streams, *Frontiers in Water*, 5, 1227167, <https://doi.org/10.3389/frwa.2023.1227167>, 2023.
- France-Lanord, C. and Derry, L. A.: Organic carbon burial forcing of the carbon cycle from Himalayan erosion, *Nature*, 390, 65–67, <https://doi.org/10.1038/36324>, 1997.
- Freeman, K. H. and Colarusso, L. A.: Molecular and isotopic records of C4 grassland expansion in the late Miocene, *Geochim. Cosmochim. Ac.*, 65, 1439–1454, [https://doi.org/10.1016/s0016-7037\(00\)00573-1](https://doi.org/10.1016/s0016-7037(00)00573-1), 2001.
- Galy, V., France-Lanord, C., and Lartiges, B.: Loading and fate of particulate organic carbon from the Himalaya to the Ganga-Brahmaputra delta, *Geochim. Cosmochim. Ac.*, 72, 1767–1787, <https://doi.org/10.1016/j.gca.2008.01.027>, 2008.

- Galy, V., Eglinton, T., France-Lanord, C., and Sylva, S.: The provenance of vegetation and environmental signatures encoded in vascular plant biomarkers carried by the Ganges–Brahmaputra rivers, *Earth Planet. Sc. Lett.*, 304, 1–12, <https://doi.org/10.1016/j.epsl.2011.02.003>, 2011.
- Galy, V., Peucker-Ehrenbrink, B., and Eglinton, T.: Global carbon export from the terrestrial biosphere controlled by erosion, *Nature*, 521, 204–207, <https://doi.org/10.1038/nature14400>, 2015.
- Garcia, C., Laronne, J. B., and Sala, M.: Variable source areas of bedload in a gravel-bed stream, *J. Sediment. Res.*, 69, 27–31, 1999.
- Garcin, Y., Schefuß, E., Schwab, V. F., Garreta, V., Gleixner, G., Vincens, A., Todou, G., Séné, O., Onana, J.-M., Achoundong, G., and Sachse, D.: Reconstructing C 3 and C 4 vegetation cover using *n*-alkane carbon isotope ratios in recent lake sediments from Cameroon, Western Central Africa, *Geochim. Cosmochim. Ac.*, 142, 482–500, <https://doi.org/10.1016/j.gca.2014.07.004>, 2014.
- Golombek, N., Scheingross, J. S., Repasch, M. N., Hovius, N., Sachse, D., Lupker, M., Eglinton, T. I., Menges, J., Haghipour, N., Poulson, S. R., Gröcke, D. R., Latosinski, F. G., and Szupiany, R. N.: Seasonal variability of fluvial organic carbon composition between 2016–2018 in the Río Bermejo, Argentina, <https://doi.org/10.1594/PANGAEA.932558>, 2021.
- Hage, S., Galy, V. V., Cartigny, M. J. B., Acikalin, S., Clare, M. A., Gröcke, D. R., Hilton, R. G., Hunt, J. E., Lintern, D. G., McGhee, C. A., Parsons, D. R., Stacey, C. D., Sumner, E. J., and Talling, P. J.: Efficient preservation of young terrestrial organic carbon in sandy turbidity-current deposits, *Geology*, 48, 882–887, <https://doi.org/10.1130/g47320.1>, 2020.
- Hage, S., Galy, V. V., Cartigny, M. J. B., Heerema, C., Heijnen, M. S., Acikalin, S., Clare, M. A., Giesbrecht, I., Gröcke, D. R., Hendry, A., Hilton, R. G., Hubbard, S. M., Hunt, J. E., Lintern, D. G., McGhee, C., Parsons, D. R., Pope, E. L., Stacey, C. D., Sumner, E. J., Tank, S., and Talling, P. J.: Turbidity currents can dictate organic carbon fluxes across river-fed fjords: An example from Bute Inlet (BC, Canada), *J. Geophys. Res.-Biogeo.*, 127, e2022JG006824, <https://doi.org/10.1029/2022jg006824>, 2022.
- Hayes, J. M., Strauss, H., and Kaufman, A. J.: The abundance of ¹³C in marine organic matter and isotopic fractionation in the global biogeochemical cycle of carbon during the past 800 Ma, *Chem. Geol.*, 161, 103–125, [https://doi.org/10.1016/S0009-2541\(99\)00083-2](https://doi.org/10.1016/S0009-2541(99)00083-2), 1999.
- Heijnen, M. S., Clare, M. A., Cartigny, M. J. B., Talling, P. J., Hage, S., Pope, E. L., Bailey, L., Sumner, E., Lintern, D. G., Stacey, C., Parsons, D. R., Simmons, S. M., Chen, Y., Hubbard, S. M., Eggenhuisen, J. T., Kane, I., and Hughes Clarke, J. E.: Fill, flush or shuffle: How is sediment carried through submarine channels to build lobes?, *Earth Planet. Sc. Lett.*, 584, 117481, <https://doi.org/10.1016/j.epsl.2022.117481>, 2022.
- Hemingway, J. D., Schefuß, E., Dinga, B. J., Pryer, H., and Galy, V. V.: Multiple plant-wax compounds record differential sources and ecosystem structure in large river catchments, *Geochim. Cosmochim. Ac.*, 184, 20–40, <https://doi.org/10.1016/j.gca.2016.04.003>, 2016.
- Hijmans, R. J., Cameron, S. E., Parra, J. L., Jones, P. G., and Jarvis, A.: Very high resolution interpolated climate surfaces for global land areas, *Int. J. Climatol.*, 25, 1965–1978, <https://doi.org/10.1002/joc.1276>, 2005.
- Hilton, R. G. and West, A. J.: Mountains, erosion and the carbon cycle, *Nature Reviews Earth & Environment*, 1, 284–299, <https://doi.org/10.1038/s43017-020-0058-6>, 2020.
- Hilton, R. G., Galy, A., and Hovius, N.: Riverine particulate organic carbon from an active mountain belt: Importance of landslides, *Global Biogeochem. Cy.*, 22, GB1017, <https://doi.org/10.1029/2006gb002905>, 2008.
- Hilton, R. G., Galy, A., Hovius, N., Hornig, M.-J., and Chen, H.: Efficient transport of fossil organic carbon to the ocean by steep mountain rivers: An orogenic carbon sequestration mechanism, *Geology*, 39, 71–74, <https://doi.org/10.1130/g31352.1>, 2011.
- Hilton, R. G., Galy, A., Hovius, N., Kao, S.-J., Hornig, M.-J., and Chen, H.: Climatic and geomorphic controls on the erosion of terrestrial biomass from subtropical mountain forest, *Global Biogeochem. Cy.*, 26, 3, <https://doi.org/10.1029/2012gb004314>, 2012.
- Hoffmann, B., Feakins, S. J., Bookhagen, B., Olen, S. M., Adhikari, D. P., Mainali, J., and Sachse, D.: Climatic and geomorphic drivers of plant organic matter transport in the Arun River, E Nepal, *Earth Planet. Sc. Lett.*, 452, 104–114, <https://doi.org/10.1016/j.epsl.2016.07.008>, 2016.
- Hoover, T. M., Marczak, L. B., Richardson, J. S., and Yonemitsu, N.: Transport and settlement of organic matter in small streams, *Freshwater Biol.*, 55, 436–449, <https://doi.org/10.1111/j.1365-2427.2009.02292.x>, 2010.
- Hou, J., D’Andrea, W. J., and Huang, Y.: Can sedimentary leaf waxes record D/H ratios of continental precipitation? Field, model, and experimental assessments, *Geochim. Cosmochim. Ac.*, 72, 3503–3517, <https://doi.org/10.1016/j.gca.2008.04.030>, 2008.
- Huang, Y., Clemens, S. C., Liu, W., Wang, Y., and Prell, W. L.: Large-scale hydrological change drove the late Miocene C4 plant expansion in the Himalayan foreland and Arabian Peninsula, *Geology*, 35, 531–534, <https://doi.org/10.1130/g23666a.1>, 2007.
- Iroumé, A., Ruiz-Villanueva, V., and Salas-Coliboro, S.: Fluvial transport of coarse particulate organic matter in a coastal mountain stream of a rainy-temperate evergreen broadleaf forest in southern Chile, *Earth Surf. Proc. Land.*, 45, 3216–3230, <https://doi.org/10.1002/esp.4961>, 2020.
- Kao, S.-J., Hilton, R. G., Selvaraj, K., Dai, M., Zehetner, F., Huang, J.-C., Hsu, S.-C., Sparkes, R., Liu, J. T., Lee, T.-Y., Yang, J.-Y. T., Galy, A., Xu, X., and Hovius, N.: Preservation of terrestrial organic carbon in marine sediments offshore Taiwan: mountain building and atmospheric carbon dioxide sequestration, *Earth Surf. Dynam.*, 2, 127–139, <https://doi.org/10.5194/esurf-2-127-2014>, 2014.
- KC Denmark A/S: Helley-Smith Sampler, <https://www.kc-denmark.dk/products/sediment-trap-station/helley-smith-sampler.aspx>, last access: 20 September 2023.
- Lee, H., Galy, V., Feng, X., Ponton, C., Galy, A., France-Lanord, C., and Feakins, S. J.: Sustained wood burial in the Bengal Fan over the last 19 My, *P. Natl. Acad. Sci. USA*, 116, 22518–22525, <https://doi.org/10.1073/pnas.1913714116>, 2019.
- Liu, J. T., Kao, S. J., Huh, C. A., and Hung, C. C.: Gravity flows associated with flood events and carbon burial: Taiwan as instructional source area, *Annu. Rev. Mar. Sci.*, 5, 47–68, <https://doi.org/10.1146/annurev-marine-121211-172307>, 2013.
- Liu, Z., Zhao, Y., Colin, C., Stattegger, K., Wiesner, M. G., Huh, C.-A., Zhang, Y., Li, X., Sompongchaiyakul, P., You,

- C.-F., Huang, C.-Y., Liu, J. T., Siringan, F. P., Le, K. P., Sathiamurthy, E., Hantoro, W. S., Liu, J., Tuo, S., Zhao, S., Zhou, S., He, Z., Wang, Y., Bunsomboonsakul, S., and Li, Y.: Source-to-sink transport processes of fluvial sediments in the South China Sea, *Earth-Sci. Rev.*, 153, 238–273, <https://doi.org/10.1016/j.earscirev.2015.08.005>, 2016.
- McArthur, A. D., Kneller, B. C., Wakefield, M. I., Souza, P. A., and Kuchle, J.: Palynofacies classification of the depositional elements of confined turbidite systems: Examples from the Gres d'Annot, SE France, *Mar. Petrol. Geol.*, 77, 1254–1273, <https://doi.org/10.1016/j.marpetgeo.2016.08.020>, 2016.
- McGlue, M. M., Smith, P. H., Zani, H., Silva, A., Carrapa, B., Cohen, A. S., and Pepper, M. B.: An Integrated Sedimentary Systems Analysis of the Rio Bermejo (Argentina): Megafan Character in the Overfilled Southern Chaco Foreland Basin, *J. Sediment. Res.*, 86, 1359–1377, <https://doi.org/10.2110/jsr.2016.82>, 2016.
- Merten, E. C., Vaz, P. G., Decker-Fritz, J. A., Finlay, J. C., and Stefan, H. G.: Relative importance of breakage and decay as processes depleting large wood from streams, *Geomorphology*, 190, 40–47, <https://doi.org/10.1016/j.geomorph.2013.02.006>, 2013.
- NASA EOSDIS Land Processes DAAC: ASTER Global Digital Elevation Model NetCDF V003, NASA EOSDIS Land Processes DAAC, https://doi.org/10.5067/MEaSURES/NASADEM/NASADEM_NC.001, 2019.
- Nichols, G. J., Cripps, J. A., Collinson, M. E., and Scott, A. C.: Experiments in waterlogging and sedimentology of charcoal: results and implications, *Palaeogeogr. Palaeoclimatol.*, 164, 43–56, [https://doi.org/10.1016/S0031-0182\(00\)00174-7](https://doi.org/10.1016/S0031-0182(00)00174-7), 2000.
- Nieto-Moreno, V., Rohrmann, A., van der Meer, M. T. J., Sinninghe Damsté, J. S., Sachse, D., Tofelde, S., Niedermeyer, E. M., Strecker, M. R., and Mulch, A.: Elevation-dependent changes in *n*-alkane δD and soil GDGTs across the South Central Andes, *Earth Planet. Sc. Lett.*, 453, 234–242, <https://doi.org/10.1016/j.epsl.2016.07.049>, 2016.
- Parsons, D. R., Jackson, P. R., Czuba, J. A., Engel, F. L., Rhoads, B. L., Oberg, K. A., Best, J. L., Mueller, D. S., Johnson, K. K., and Riley, J. D.: Velocity Mapping Toolbox (VMT): a processing and visualization suite for moving-vessel ADCP measurements, *Earth Surf. Proc. Land.*, 38, 1244–1260, <https://doi.org/10.1002/esp.3367>, 2013.
- Ponton, C., West, A. J., Feakins, S. J., and Galy, V.: Leaf wax biomarkers in transit record river catchment composition, *Geophys. Res. Lett.*, 41, 6420–6427, <https://doi.org/10.1002/2014gl061328>, 2014.
- Powell, R. L., Zoo, E.-H., and Still, C. J.: Vegetation and soil carbon-13 isoscapes for South America integrating remote sensing and ecosystem isotope measurements, *Ecosphere*, 3, 109, <https://doi.org/10.1890/ES12-00162.1>, 2012.
- Rach, O., Hadeen, X., and Sachse, D.: An automated solid phase extraction procedure for lipid biomarker purification and stable isotope analysis, *Org. Geochem.*, 142, 103995, <https://doi.org/10.1016/j.orggeochem.2020.103995>, 2020.
- Reid, I., Laronne, J. B., and Powell, D. M.: Flash-flood and bedload dynamics of desert gravel-bed streams, *Hydrol. Process.*, 12, 543–557, [https://doi.org/10.1002/\(SICI\)1099-1085\(19980330\)12:4<543::AID-HYP593>3.0.CO;2-C](https://doi.org/10.1002/(SICI)1099-1085(19980330)12:4<543::AID-HYP593>3.0.CO;2-C), 1998.
- Repasch, M., Wittmann, H., Scheingross, J. S., Sachse, D., Szupiany, R., Orfeo, O., Fuchs, M., and Hovius, N.: Sediment Transit Time and Floodplain Storage Dynamics in Alluvial Rivers Revealed by Meteoric ^{10}Be , *J. Geophys. Res.-Earth*, 125, e2019JF00541, <https://doi.org/10.1029/2019jff005419>, 2020.
- Repasch, M., Scheingross, J. S., Hovius, N., Lupker, M., Wittmann, H., Haghipour, N., Gröcke, D. R., Orfeo, O., Eglinton, T. I., and Sachse, D.: Fluvial organic carbon cycling regulated by sediment transit time and mineral protection, *Nat. Geosci.*, 14, 842–848, <https://doi.org/10.1038/s41561-021-00845-7>, 2021.
- Repasch, M., Scheingross, J. S., Hovius, N., Vieth-Hillebrand, A., Mueller, C. W., Höschen, C., Szupiany, R. N., and Sachse, D.: River Organic Carbon Fluxes Modulated by Hydrodynamic Sorting of Particulate Organic Matter, *Geophys. Res. Lett.*, 49, e2021GL096343, <https://doi.org/10.1029/2021gl096343>, 2022.
- Repasch, M., Scheingross, J. S., Cook, K. L., Sachse, D., Dosch, S., Orfeo, O., and Hovius, N.: Lithospheric Flexure Controls on Geomorphology, Hydrology, and River Chemistry in the Andean Foreland Basin, *AGU Advances*, 4, e2023AV000924, <https://doi.org/10.1029/2023AV000924>, 2023.
- Rickenmann, D.: Variability of Bed Load Transport During Six Summers of Continuous Measurements in Two Austrian Mountain Streams (Fischbach and Ruetz), *Water Resour. Res.*, 54, 107–131, <https://doi.org/10.1002/2017WR021376>, 2018.
- Rohrmann, A., Strecker, M. R., Bookhagen, B., Mulch, A., Sachse, D., Pingel, H., Alonso, R. N., Schildgen, T. F., and Montero, C.: Can stable isotopes ride out the storms? The role of convection for water isotopes in models, records, and paleoaltimetry studies in the central Andes, *Earth Planet. Sc. Lett.*, 407, 187–195, <https://doi.org/10.1016/j.epsl.2014.09.021>, 2014.
- Ruiz-Villanueva, V., Mazzorana, B., Bladé, E., Bürkli, L., Iribarren-Anacona, P., Mao, L., Nakamura, F., Ravazzolo, D., Rickenmann, D., Sanz-Ramos, M., Stoffel, M., and Wohl, E.: Characterization of wood-laden flows in rivers, *Earth Surf. Proc. Land.*, 44, 1694–1709, <https://doi.org/10.1002/esp.4603>, 2019.
- Sachse, D., Radke, J., and Gleixner, G.: Hydrogen isotope ratios of recent lacustrine sedimentary *n*-alkanes record modern climate variability, *Geochim. Cosmochim. Ac.*, 68, 4877–4889, <https://doi.org/10.1016/j.gca.2004.06.004>, 2004.
- Sachse, D., Billault, I., Bowen, G. J., Chikaraishi, Y., Dawson, T. E., Feakins, S. J., Freeman, K. H., Magill, C. R., McInerney, F. A., van der Meer, M. T. J., Polissar, P., Robins, R. J., Sachs, J. P., Schmidt, H.-L., Sessions, A. L., White, J. W. C., West, J. B., and Kahmen, A.: Molecular Paleohydrology: Interpreting the Hydrogen-Isotopic Composition of Lipid Biomarkers from Photosynthesizing Organisms, *Annu. Rev. Earth Pl. Sc.*, 40, 221–249, <https://doi.org/10.1146/annurev-earth-042711-105535>, 2012.
- Sambrook Smith, G. H., Best, J. L., Leroy, J. Z., Orfeo, O., and Baas, J.: The alluvial architecture of a suspended sediment dominated meandering river: the Río Bermejo, Argentina, *Sedimentology*, 63, 1187–1208, <https://doi.org/10.1111/sed.12256>, 2016.
- Schefuss, E., Schouten, S., and Schneider, R. R.: Climatic controls on central African hydrology during the past 20 000 years, *Nature*, 437, 1003–1006, <https://doi.org/10.1038/nature03945>, 2005.
- Scheingross, J. S., Hovius, N., Dellinger, M., Hilton, R. G., Repasch, M., Sachse, D., Gröcke, D. R., Vieth-Hillebrand, A., and Turowski, J. M.: Preservation of organic carbon during active fluvial transport and particle abrasion, *Geology*, 47, 958–962, <https://doi.org/10.1130/g46442.1>, 2019.

- Scheingross, J. S., Repasch, M. N., Hovius, N., Sachse, D., Lupker, M., Fuchs, M., Halevy, I., Gröcke, D. R., Golombek, N. Y., Haghypour, N., Eglinton, T. I., Orfeo, O., and Schleicher, A. M.: The fate of fluvially-deposited organic carbon during transient floodplain storage, *Earth Planet. Sc. Lett.*, 561, 116822, <https://doi.org/10.1016/j.epsl.2021.116822>, 2021.
- Schlünz, B. and Schneider, R. R.: Transport of terrestrial organic carbon to the oceans by rivers: re-estimating flux- and burial rates, *Int. J. Earth Sci.*, 88, 599–606, <https://doi.org/10.1007/s005310050290>, 2000.
- Schwab, M. S., Hilton, R. G., Haghypour, N., Baronas, J. J., and Eglinton, T. I.: Vegetal Undercurrents – Obscured Riverine Dynamics of Plant Debris, *J. Geophys. Res.-Biogeo.*, 127, e2021JG006726, <https://doi.org/10.1029/2021jg006726>, 2022.
- Selva, E. C., Couto, E. G., Johnson, M. S., and Lehmann, J.: Litterfall production and fluvial export in headwater catchments of the southern Amazon, *J. Trop. Ecol.*, 23, 329–335, <https://doi.org/10.1017/s0266467406003956>, 2007.
- Seo, J. I., Nakamura, F., Nakano, D., Ichiyanagi, H., and Chun, K. W.: Factors controlling the fluvial export of large woody debris, and its contribution to organic carbon budgets at watershed scales, *Water Resour. Res.*, 44, W04428, <https://doi.org/10.1029/2007wr006453>, 2008.
- Silva, L. C. R., Giorgis, M. A., Anand, M., Enrico, L., Pérez-Harguindeguy, N., Falczuk, V., Tieszen, L. L., and Cabido, M.: Evidence of shift in C4 species range in central Argentina during the late Holocene, *Plant Soil*, 349, 261–279, <https://doi.org/10.1007/s11104-011-0868-x>, 2011.
- Smith, J. A., Mazumder, D., Suthers, I. M., Taylor, M. D., and Bowen, G.: To fit or not to fit: evaluating stable isotope mixing models using simulated mixing polygons, *Methods Ecol. Evol.*, 4, 612–618, <https://doi.org/10.1111/2041-210x.12048>, 2013.
- Smith, J. C., Galy, A., Hovius, N., Tye, A. M., Turowski, J. M., and Schleppe, P.: Runoff-driven export of particulate organic carbon from soil in temperate forested uplands, *Earth Planet. Sc. Lett.*, 365, 198–208, <https://doi.org/10.1016/j.epsl.2013.01.027>, 2013.
- Sparkes, R. B., Lin, I.-T., Hovius, N., Galy, A., Liu, J. T., Xu, X., and Yang, R.: Redistribution of multi-phase particulate organic carbon in a marine shelf and canyon system during an exceptional river flood: Effects of Typhoon Morakot on the Gaoping River–Canyon system, *Mar. Geol.*, 363, 191–201, <https://doi.org/10.1016/j.margeo.2015.02.013>, 2015.
- Stallard, R. F.: Terrestrial sedimentation and the carbon cycle: Coupling weathering and erosion to carbon burial, *Global Biogeochem. Cy.*, 12, 231–257, <https://doi.org/10.1029/98gb00741>, 1998.
- Stewart, M. K. and Taylor, C. B.: Environmental isotopes in New Zealand hydrology; 1 Introduction The role of oxygen-18, deuterium, and tritium in hydrology, *New Zeal. J. Sci.*, 24, 295–311, 1981.
- Thomas, C. L., Jansen, B., van Loon, E. E., and Wiesenberg, G. L. B.: Transformation of *n*-alkanes from plant to soil: a review, *SOIL*, 7, 785–809, <https://doi.org/10.5194/soil-7-785-2021>, 2021.
- Turowski, J. M., Rickenmann, D., and Dadson, S. J.: The partitioning of the total sediment load of a river into suspended load and bedload: a review of empirical data, *Sedimentology*, 57, 1126–1146, <https://doi.org/10.1111/j.1365-3091.2009.01140.x>, 2010.
- Turowski, J. M., Badoux, A., Bunte, K., Rickli, C., Federspiel, N., and Jochner, M.: The mass distribution of coarse particulate organic matter exported from an Alpine headwater stream, *Earth Surf. Dynam.*, 1, 1–11, <https://doi.org/10.5194/esurf-1-1-2013>, 2013.
- Turowski, J. M., Hilton, R. G., and Sparkes, R.: Decadal carbon discharge by a mountain stream is dominated by coarse organic matter, *Geology*, 44, 27–30, <https://doi.org/10.1130/g37192.1>, 2016.
- Tyson, R. V. and Follows, B.: Palynofacies prediction of distance from sediment source – A case study from the Upper Cretaceous of the Pyrenees, *Geology*, 28, 569–571, 2000.
- Walker, C. D. and Richardson, S. B.: The use of stable isotopes of water in characterising the source of water in vegetation, *Chemical Geology: Isotope Geoscience section*, 94, 145–158, [https://doi.org/10.1016/0168-9622\(91\)90007-J](https://doi.org/10.1016/0168-9622(91)90007-J), 1991.
- West, A. J., Lin, C. W., Lin, T. C., Hilton, R. G., Liu, S. H., Chang, C. T., Lin, K. C., Galy, A., Sparkes, R. B., and Hovius, N.: Mobilization and transport of coarse woody debris to the oceans triggered by an extreme tropical storm, *Limnol. Oceanogr.*, 56, 77–85, <https://doi.org/10.4319/lo.2011.56.1.0077>, 2011.
- Wohl, E., Ogden, F. L., and Goode, J.: Episodic wood loading in a mountainous neotropical watershed, *Geomorphology*, 111, 149–159, <https://doi.org/10.1016/j.geomorph.2009.04.013>, 2009.
- Wohl, E., Kramer, N., Ruiz-Villanueva, V., Scott, D. N., Comiti, F., Gurnell, A. M., Piegay, H., Lininger, K. B., Jaeger, K. L., Walters, D. M., and Fausch, K. D.: The Natural Wood Regime in Rivers, *BioScience*, 69, 259–273, <https://doi.org/10.1093/biosci/biz013>, 2019.
- Yager, E. M., Turowski, J. M., Rickenmann, D., and McArdeall, B. W.: Sediment supply, grain protrusion, and bedload transport in mountain streams, *Geophys. Res. Lett.*, 39, L10402, <https://doi.org/10.1029/2012gl051654>, 2012.